Scientific Voyage
Vol. 2, No. 1,
Page 1-10 (2021)

SCIENTIFIC VOYAGE
ISSN: 2395-5546

GCECT
Publication
Jan.-Mar.

Transition metal doped hydroxyapatites: from chemistry to antibacterial properties

Arjak Bhattacharjee[1a]

Department of Ceramic Technology, Government College of Engineering and Ceramic Technology, Kolkata 700010, W.B., India

Abstract. Musculoskeletal disorders are one of the leading causes of disability. Currently, 1.3 billion population across the globe are suffering from various musculoskeletal disorders (MSK) and it imposes a total of $ 136.8 billion annual burden to the US economy. Current treatment options consist of pain medication and surgical intervention by inserting implants and scaffolds on the affected site. Hydroxyapatite [HA, $Ca_{10}(PO_4)_6OH_2$] based implants are widely preferred for tissue engineering applications due to their compositional similarities with human bone. However, post-surgical infections on the implant surface often cause implant failure and need to be rectified by three times costlier revision surgery. The flexible crystal chemistry of hydroxyapatite allows transition metal substitution both in the cationic and anionic sites due to the ionic radius differences between calcium and first row transition metals. Transition metal substitutions incorporate exiting biological and antibacterial properties to HA. This paper will summarize the available literature reports which describe the crystal chemistry of first row transition metal incorporation in HA and the resulting antibacterial properties.

Keywords: Hydroxyapatite, transition metal doping, Antibacterial efficacy, crystal chemistry

1. Introduction and historical background

1944! It was the story of devastated Europe during world war two. A Jew young man was able to escape from the holocaust and took refuge in Institute of soil research to continue the studies of Apatite minerals which he had started in Scandanavia [1-3]. Figure 1is a tribute to that young man, named Victor Goldschmidt, who is known as the father of modern geochemistry. Apatites (A10(MO4)6X2) are a diverse family of materials which have attracted wide attention in the scientific community due to their broad application as pigments, catalyst, energy materials, materials for the remediation of hazardous waste and as a bio-ceramics [4-8]. The general chemical formula of apatite is A10(PO4)6X2 where the A cation can be an alkaline earth metal

[a] **Present address:** *School of Mechanical and Materials Engineering, Washington State University, Pullman, WA, USA*

[1] Email: arjak.ceramic16@gmail.com

Sr, Ca or Ba and the X anion can be OH^- ion or Cl^- ion, which represents hydroxyapatite, and chlorapatite, respectively. V. Goldschmidt was the first one in history who explained apatite structures by thorough study of deposits in Scandinavia. That time apatite structure was represented by the general notation [Ca4][Ca6][(PO4)6][F]2, which represents that it is formed CaO6 units and those are joined together with PO4 networks which make a structure similar to that of a hexagonal honeycomb extending in the c direction [9-11].

Why could bone take up fluorine selectively even from dilute solutions? This was one of the most wondering questions to scientists of that era. A careful examination of apatite structure gave a satisfactory answer to this question and the following conclusion was reached based on the observations and experimental results. (1) apatite structure is a channel structure with partitions having corner-connected CaO_6 and PO_4 polyhedra; (2) bond-length criteria are fulfilled with filling of these channels by Ca and anions (OH^-, F^-); and (3) change in channel length happens with variation of ionic radii. Keeping these factors in consideration, better stability of Fluroapatite can be explained by the best fit of fluorine atom in apatite structure which is the basic science behind the treatment of dental cavities by altering fluorine content [12,13].

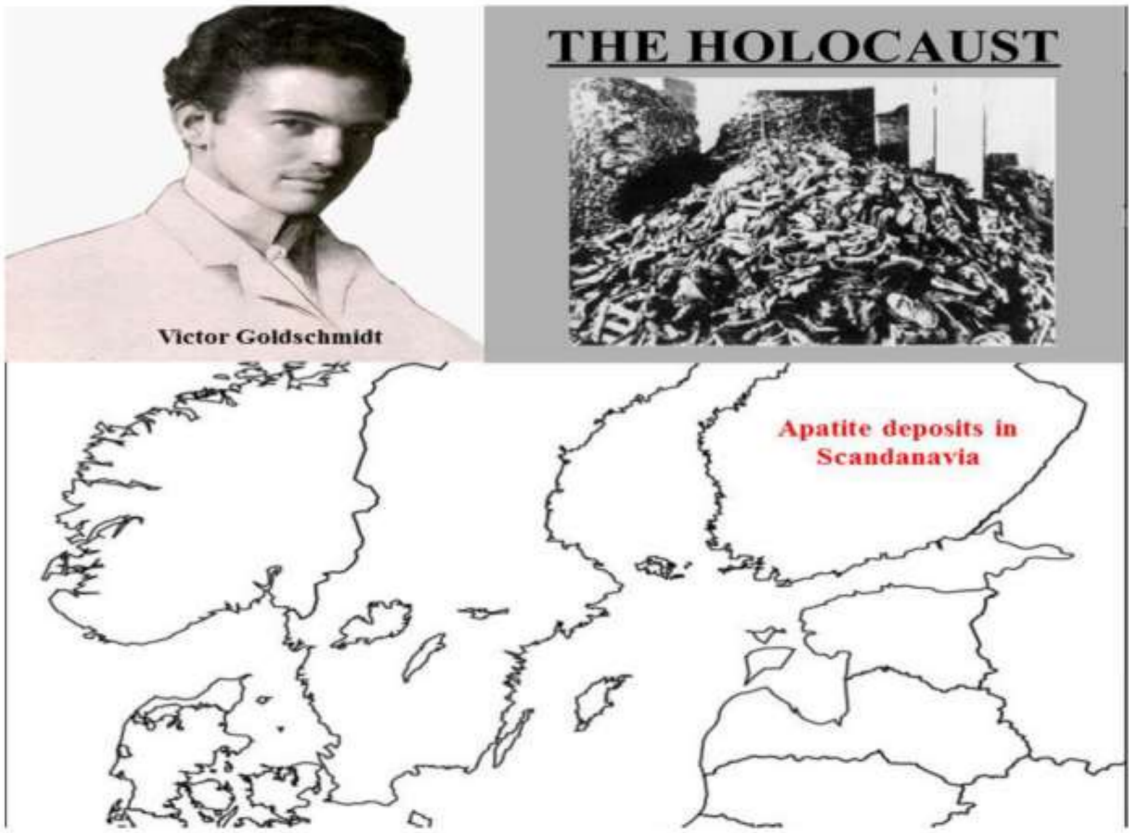

Fig. 1: History of research on apatite crystal chemistry

Calcium hydroxyapatite [HA, $Ca_{10}(PO_4)_6OH_2$], an important member of the apatite family is a suitable ceramic for orthopedic, dental, and maxillofacial repair [14–16] due to its hexagonal structure and Ca/P ratio of 1.67, that identical to bone apatite. To tailor the crystal chemistry of HA for specific applications (bioceramic, catalyst, pigments etc.), doping with several transition metals are a unique option [17,18]. Doping of HA by metals like Ag, Cu and Zn also improves its biological properties. However, to understand the doping mechanism of cations in HA structure and its effect on chemical and biological properties, it is very important to demonstrate the effect of processing techniques via solid state route, wet chemical routes and heat treatment cycleon doping mechanism [19-20].

2. The open debate about transition metal doping site in hydroxyapatite

Several contradictory reports are presented in literature regarding doping site of transition metals in HA structure. It can be concluded from the available literature that when sintering temperature is above 900 °C, Zn^{+2} ions not simply substitute the Ca site of HA instead they reside in the OH hexagonal channel [21]. Similar phenomena have been observed in case of Cu after heat treatment and quenching from 1100 °C [22]. But now the question comes, *why is this happening? Is it possible to incorporate transition metals in OH channel instead of Ca site?* A detailed investigation about at ionic radii parameters of concerned ions indicate that there is a large difference of ionic radii value (~25%) between Ca^{2+} and transition metal cations as listed in table 1. This is the primary reason why transition metals are not always substitutes in the cationic site of HA [23].

Element	Coordination no.	Ionic radius (Å)
Ca^{+2}	8 (octaheadral)	1.00
Mn^{+2}	8 (octaheadral)	0.67
Co^{+2}	8 (octaheadral)	0.65
Ni^{+2}	8 (octaheadral)	0.69
Cu^{+2}	8 (octaheadral)	0.73
Zn^{+2}	8 (octaheadral)	0.74

Table 1: Ionic radius comparison of Ca^{+2} and first row transition metals

Correlation of heat treatment parameters with Rietveld refinement data of doped samples revealed that below a temperature of 700 °C, Zn^{+2} incorporation happens in b-TCP structure of the biphasic calcium phosphate which leads to unit cell volume contraction. When the sintering temperature is above 900 °C, then b-TCP becomes unstable and Zn^{+2} incorporation happens in the interstitial 2b wyckoff position instead of the Ca site which leads to unit cell volume expansion of doped hydroxyapatite [24]. A similar observation has been found for Cu^{+2} when the sintering temperature reaches above 1100 °C [25]. However, Cu^{+2} show a tendency of reduction to Cu^{+1} when heated at that temperature. No such observation (tendency of reduction) had been found in case of Zn^{+2}. Figures 2 represents the crystal structure of pure HA with different crystallographic sites.

3. Effects of Copper doping in HA

3.1 Effect on HA crystal chemistry

As discussed in the earlier sections, Cu can go both in Ca site of HA structure as well as in OH channel depending on the preparation techniques. According to the available literature, if copper doping in HA is performed in solid state reaction route followed by quenching from 1100 °C, Cu goes in OH channels retaining the hexagonal crystal structure with space group *P*63/*m* [21]. Logically it can be concluded from table 1, due to the smaller size of Cu^{+2} (~0.73 Å) in comparison to Ca^{+2} (~1.00 Å), unit cell volume reduction will happen for substitution of Cu^{+2} in Ca^{+2} position of HA structure. However, opposite observation was found after heat treatment and quenching from 1100 °C (it leads to incorporation of Cu in OH channel of HA instead Ca site). substitution in OH

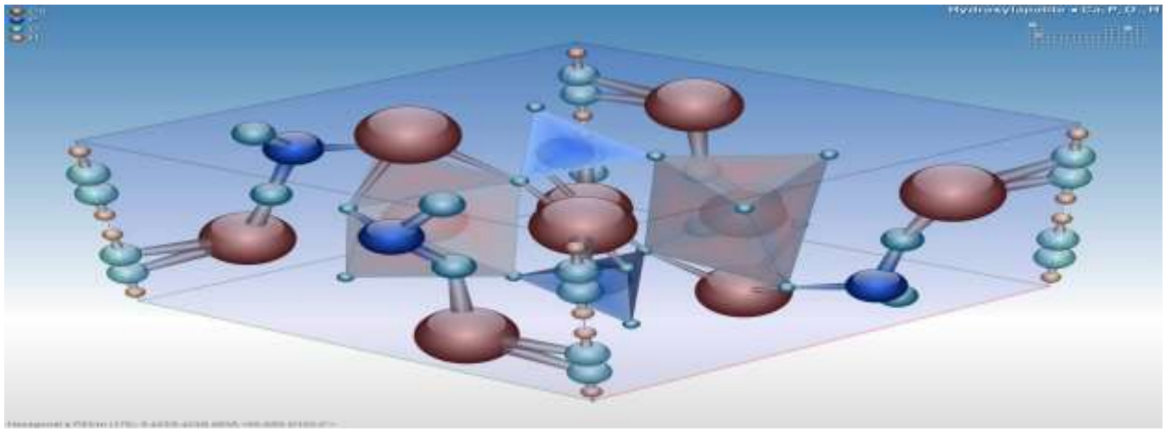

Fig. 2: Crystal structure model of HA [26]

channel. A previous work reports the Xray absorption spectroscopy (XAS) result of Cu doped HA containing Cu in OH channels. It is previously reported that heat treatment over 1100 °C leads to reduction of Cu^{+2} to Cu^{+1} (peak around 8990 eV) [21]. Due to the mixed oxidation states of Cu in HA, it results in O-Cu-O chromophore with bright pink color [27]. The presence of these chromophores makes Cu doped HA, a potential candidate for use as an inert non-toxic pigment that is stable even at high temperatures.

3.2 Effects on biological properties of HA

Due to its involvement in several metabolic processes, Cu is an essential micronutrient of several living organisms. However, due to its ability to form reactive oxygen species, the cytotoxicity limit of Cu is an important factor that needs serious attention [28]. The antimicrobial properties of copper were known since ancient times and examples can be found in ancient Indian literatures where uses of Cu as drinking water sterilizing metal has been reported [29.30]. Figure 3 represents various uses of Cu in different parts of India.

Fig. 3: Uses of Cu in different parts of India

There are various competing theories to explain the antibacterial mechanism of Cu. Although no theory can explain it with perfection [30]. The most accepted theory is that Cu causes reduction potential change of bacterial cell membrane followed by its penetration inside the cell. Cu has the ability to forms reactive oxygen species as well as it can bond with the thiol, amine and carboxyl groups present inside the cell. Combinations of these two effects cause cell

membrane dysfunction which is the major cause of cell death. Several researchers also demonstrated that Cu forms bond with the DNA of bacterial cell causing DNA damage and leads to cell death [31,32]. Variable oxidation states of Cu are also an important factor to determine its antimicrobial efficiency. It has been reported that Cu^{+1} is more toxic to bacteria than Cu^{+2} [21]. A previous work also reports that due to leaching of Cu from HA structure (~0.082 ppm to 0.73 ppm in PBS solution for a doping level of 1 wt. % and 10 wt. % respectively), Cu doped HA shows zone of inhibition ranging from 0.2 cm to 0.5 cm [33]. However, most antimicrobial studies of Cu doped HA were performed after substituting Cu in Ca site of HA and confirming Cu^{+2} oxidation state. One recent study concludes that Cu can also show antibacterial property after getting incorporated inside the hydroxyl channels.

4. Effects of Zinc doping in HA

4.1 Effect on HA crystal chemistry

Available literature on Zn doped HA suggests that without any heat treatment operation in wet chemical route, Zn^{+2} is incorporated in Ca site of HA [24]. However, heat treatment at 1100 °C results incorporation of Zn^{+2} in the hexagonal channel of HA structure at the 2b Wyckoff site and forms O–Zn–O bonding [22], which results to a solid solution of the formula $Ca_{10}Zn_x(PO_4)_6(OH)_{2-2x}O_{2x}$. Incorporation of Zn^{+2} in OH channel happens due to the more stable HA phase at 1100 °C thanb-TCP. Insertion of Zn^{+2} is similar to that of Cu^{+2} but Zn^{+2} does not show any change of oxidation states as shown for Cu.

4.2. Effect of Zn doping on Biological properties of HA

It also been proved that Zn^{+2} shows antimicrobial properties against a wide range of bacteria (*S. aureus, E. coli*, *S. epidermidis*) and other microorganisms (*c. albican*). Most studies of Zn doped HA have been performed after substituting Zn in Ca site of HA structure [34]. Nowdays it is of utmost importance to understand the effect of Zn substitution site on the antibacterial efficiency of Zn doped HA. One recent work report that Zn substitution in the OH channels does not show any antibacterial effects against E. coli and S. aureus due to restricted Zn leaching by the formation of O-Zn-O bonding. Figure 4 represents the antibacterial mechanism of Zn doped hydroxyapatite after substitution in different doping sites.

5. Summary and future trends

This paper summarizes that, (1) The substitution site of Cu and Zn in HA structure can be altered by altering the processing parameters (heat treatment cycle, doping composition in solid state and wet chemical processing route etc.). For doping Cu in HA by solid state route, there is a confirmation that Cu goes into the HA channel after heat treatment. (2) Most of the antibacterial

Cu doped HA are prepared by wet chemical route confirming the substitution of Cu in Ca site of HA. Antibacterial efficiency of Cu substituted HA [Cu in OH channel of HA] prepared by wet chemical route also demonstrates antibacterial efficacy. In contrast, the Zn doped HA shows antibacterial efficacy only when Zn replaces the Ca site of the HA. (3) Zn can be doped in HA by wet chemical route and there is evidence to confirm that incorporation of Zn in OH channel of HA structure happens heat treatment at 1100 °C, but this substitution leads to restricted Zn leaching and no antibacterial efficacy due to the formation of O-Zn-O binding. Future works in this field can be directed to (a) to test the cytotoxicity of Cu and Zn doped HA with human osteoblast cells for monitoring the maximum safety doping limit of Cu and Zn in HA (b) to find out which method of synthesis (between solid state and wet chemical) is better for production of less toxic Cu and Zn doped HA (c) to characterize the potential of prepared materials for using as a bone implant by in vivo testing in mouse models (d) based on the results of in vivo testing, patient specific scaffold can be prepared by the doped HA powder, using 3D printing technique (e) after analyzing 3D printing results carefully, obtained scaffolds can be utilized for low load bearing defect repair such as spinal fusion.

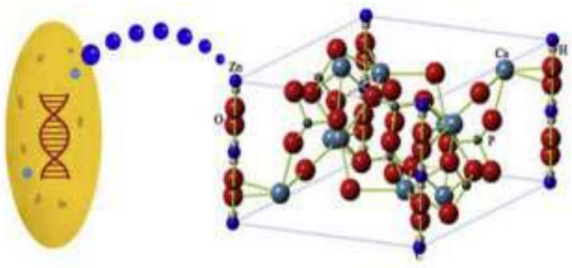

Restricted bacterial killing after thermal treatment and Zn substitution in OH channel

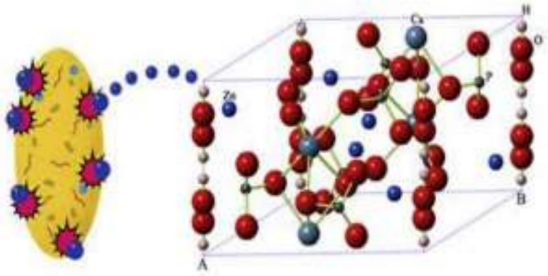

Enhanced bacterial killing after Zn substitution in Ca site of HA

Fig.4.

Schematic representing enhanced bacterial killing after Zn incorporation in Ca site of HA, whereas, Zn substitution in the OH channels leads to no bacterial killing due to restricted Zn leaching by the formation of O-Zn-O bonding [22].

Acknowledgement:

The author would like to acknowledge Prof. Kantesh Balani (IIT Kanpur), Prof. Indranil Manna (IIT Kharagpur), Prof. H.S. Maiti (CSIR-CGCRI), Prof. Timothy John White (NTU Singapore), Dr. Tom Baikie (NTU Singapore), Prof. Bikramjit Basu (IISc Bangalore) and Dr. T.K. Bhattacharya (GCECT Kolkata) for fruitful discussions and inputs on this topic.

References:

[1] V. Kahlenberg and H. Krüger, *Solid state Sci.* **6** (2004) 553.

[2] J. Felsche, *J. Solid State Chem.* **5** (1972) 266.

[3] T. White, C. Ferraris, J. Kim and S. Madhavi, *Rev. Mineral. Geochem.* **57** (2005) 307.

[4] G.B. Kauffman, *Chem. Educ.* **2** (1997) 1.

[5] D.F. Williams, *Biomaterials* **30** (2009) 5897.

[6] T.N. Kim, Q.L. Feng, J.O. Kim, J. Wu, H. Wang, G.C. Chen and F.Z. Cui, *J. Mater. Sci. Mater. Med.* **9** (1998) 129.

[7] G. Liu, J. W. Talley, C. Na, S.L. Larson and L.G. Wolfe, *Environ. Sci. Technol.* **44** (2010) 1366.

[8] S. Bailliez, A. Nzihou, E. Beche and G. Flamant, *Process Saf. Environ. Prot.*, **82** (2004) 175.

[9] D. Marrero-López, P. Díaz-Carrasco, J. Peña-Martínez, J.C. Ruiz-Morales and J.R. Ramos-Barrado, *Fuel Cells* **11** (2011) 65.

[10] Z. Dong, T.J. White, B. Wei and K. Laursen, *J. Am. Ceram. Soc.* **85** (2002) 2515.

[11] H. Nishikawa and K. Omamiuda, *J. Mol. Catal. A Chem.* **179** (2002) 193.

[12] P.R. Slater, J.E.H. Sansom and J.R. Tolchard, *Chem. Rec.* **4** (2004) 373.

[13] I. Mobasherpour, M.S. Heshajin, A. Kazemzadeh and M. Zakeri, *J. Alloys Compd.* **430**, (2007) 330.

[14] P.N. De Aza, F. Guitian, C. Santos, S. De Aza, R. Cusco and L. Artus, *Chem. Mater.* **9** (1997) 916.

[15] J.H. Shepherd, D.V Shepherd and S.M. Best, *J. Mater. Sci. Mater. Med.* **23** (2012) 2335.

[16] G. Renaudin, S. Gomes and J.-M. Nedelec, *Materials (Basel)* **10** (2017) 92.

[17] S. Gomes, C. Vichery, S. Descamps, H. Martinez, A. Kaur, A. Jacobs, J.-M. Nedelec and G. Renaudin, *Acta Biomater.* **65** (2018) 462.

[18] A.S. Karpov, J. Nuss, M. Jansen, P.E. Kazin and Y.D. Tretyakov, *Solid State Sci.* **5** (2003) 1277.

[19] S. Ben Moussa, J. Lachheb, M. Gruselle, B. Maaten, K. Kriis, T. Kanger, K. Tõnsuaadu and B. Badraoui, *Tetrahedron* **73** (2017) 6542.

[20] S. Moonga and D.W. Dempster, *J. Bone Miner. Res.* **10** (1995) 453.

[21] A. Bhattacharjee et al. *Crystal chemistry and antibacterial properties of cupriferous hydroxyapatite. Materials* **12** (2019) 1814.

[22] A. Bhattacharjee et al., *Ceram. Int.* **45** (2019) 12225.

[23] A. Bhattacharjee, A. Gupta, M. Prem Anand, P. Sengupta, A. Pandey and T.K. Bhattacharya, *Int. J. Appl. Ceram. Technol.* **17** (2020) 327.

[24] V. Stanić, S. Dimitrijević, J. Antić-Stanković, M. Mitrić, B. Jokić, I.B. Plećaš and S. Raičević, *Appl. Surf. Sci.* **256** (2010) 6083.

[25] I. Dragieva, S. Stoeva, P. Stoimenov, E. Pavlikianov and K. Klabunde, *Nanostructured Mater.* **12** (1999) 267.

[26] A. Bhattacharjee, *Ame. Ceram. Soc. Bull.* **97** (2018) 31.

[27] T. Baikie, G.M.H. Ng, S. Madhavi, S.S. Pramana, K. Blake, M. Elcombe and T.J. White, *Dalt. Trans.* (2009) 6722.

[28] S. Gomes, C. Vichery, S. Descamps, H. Martinez, A. Kaur, A. Jacobs, J.-M. Nedelec and G. Renaudin, *Acta Biomater.* **65** (2018) 462.

[29] S. Mathews, M. Hans, F. Mücklich and M. Solioz, *Appl. Environ. Microbiol.* **79** (2013) 2605.

[30] V.G. Desai, *Bharatiya Rasashastra (The Ancient Chemistry of India)*, Gajaanan Book Depot, Bombay (1928).

[31] I. Uckay, D. Pittet, P. Vaudaux, H. Sax, D. Lew and F. Waldvogel, *Ann. Med.* **41** (2009) 109.

[32] S.I. Weinstein, E.H. Yelin and S. I. Watkins-Castillo, *The Big Picture Burden of Musculoskeletal Diseases (BMUS),* http://www.boneandjointburden.org/2014-report/i0/big-picture.

[33] Y. Li, J. Ho and C. P. Ooi, *Mater. Sci. Eng. C* **30** (2010) 1137.

Scientific Voyage
Vol. 2, No. 1,
Page 11-19 (2021)

SCIENTIFIC VOYAGE
ISSN: 2395-5546

GCECT
Publication
Jan.-Mar.

Classical Trajectories in Rindler Space

Soma Mitra[1], Sanchita Das[2] and Somenath Chakrabarty[3]
Department of Physics, Visva-Bharati, Santiniketan 731235, India

Abstract: The nature of single particle classical phase space trajectories in Rindler space with non-hermitian PT-symmetric Hamiltonian have been studied both in the relativistic as well as in the non-relativistic scenarios. It has been shown that in the relativistic scenario, both positional coordinates and the corresponding canonical momenta are real in nature and diverges with time. Whereas the phase space trajectories are a set of hyperbolas in Rindler space. On the other hand in the non-relativistic approximation the spatial coordinates are complex in nature, whereas the corresponding canonical momenta of the particle are purely imaginary. In this case the phase space trajectories are quite simple in nature. But the spatial coordinates are restricted in the negative region only.

Keywords: Rindler space; Uniformly accelerated frame; Classical trajectory; Poisson's equation

1. Introduction

Exactly like the Lorentz transformations of space time coordinates in the inertial frame [1,2], the Rindler coordinate transformations are for the uniformly accelerated frame of reference with respect to some inertial one [3–9]. From the references [3–9], it can very easily be shown that the Rindler coordinate transformations are given by

$$ct = \left(\frac{c^2}{\alpha} + x'\right)\sinh\left(\frac{\alpha t'}{c}\right) \quad \text{and}$$
$$x = \left(\frac{c^2}{\alpha} + x'\right)\cosh\left(\frac{\alpha t'}{c}\right). \tag{1}$$

Hence it is a matter of simple algebra to prove that the inverse transformations are given by

$$ct' = \frac{c^2}{2\alpha}\ln\left(\frac{x+ct}{x-ct}\right) \quad \text{and} \quad x' = (x^2 - (ct)^2)^{1/2} - \frac{c^2}{\alpha}. \tag{2}$$

Here α indicates the uniform acceleration of the frame. Hence it can very easily be shown from Eqs. (1) and (2) that the square of the four-line element changes from

$$ds^2 = d(ct)^2 - dx^2 - dy^2 - dz^2 \quad \text{to}$$
$$ds^2 = \left(1 + \frac{\alpha x'}{c^2}\right)^2 d(ct')^2 - dx'^2 - dy'^2 - dz'^2, \tag{3}$$

[1] E-mail: somaphysics@gmail.com
[2] E-mail: sanchita.das@visva-bharati.ac.in
[3] E-mail: somenath.chakrabarty@visva-bharati.ac.in

where the former line element is in the Minkowski space.

Hence the metric in the Rindler space can be written as

$$g^{\mu\nu} = \text{diag}\left(\left(1+\frac{\alpha x}{c^2}\right)^2, -1, -1, -1\right), \tag{4}$$

whereas in the Minkowski space-time we have the usual form

$$g^{\mu\nu} = \text{diag}(+1, -1, -1, -1). \tag{5}$$

It is therefore quite obvious that the Rindler space is also flat. The only difference from the Minkowski space is that the frame of the observer is moving with uniform acceleration. It has been noticed from the literature survey, that the principle of equivalence plays an important role in obtaining the Rindler coordinates in the uniformly accelerated frame of reference. According to this principle, an accelerated frame in absence of gravity is equivalent to a frame at rest in presence of a gravity. Therefore in the present scenario, α may be treated to be the strength of constant gravitational field for a frame at rest.

Now from the relativistic dynamics of special theory of relativity [1], the action integral is given by

$$S = -\alpha_0 c \int_a^b ds \equiv \int_a^b L dt, \tag{6}$$

where $\alpha_0 = -m_0 c$ [1] and m_0 is the rest mass of the particle and c is the speed of light in vacuum.

The Lagrangian of the particle may be written as

$$L = -m_0 c^2 \left[\left(1+\frac{\alpha x}{c^2}\right)^2 - \frac{v^2}{c^2}\right]^{1/2}, \tag{7}$$

where $\mathbf{v}$ is the three velocity vector. Hence the three momentum of the particle is given by

$$\mathbf{p} = \frac{\partial L}{\partial \mathbf{v}}, \quad \text{or} \tag{8}$$

$$\mathbf{p} = \frac{m_0 \mathbf{v}}{\left[\left(1+\frac{\alpha x}{c^2}\right)^2 - \frac{v^2}{c^2}\right]^{1/2}}. \tag{9}$$

Then from the definition, the Hamiltonian of the particle may be written as

$$H = \mathbf{p}.\mathbf{v} - L \quad \text{or} \tag{10}$$

$$H = m_0 c^2 \left(1+\frac{\alpha x}{c^2}\right)\left(1+\frac{p^2}{m_0^2 c^2}\right)^{1/2}. \tag{11}$$

Hence it can very easily be shown that in the non-relativistic approximation, the Hamiltonian is given by

$$H = \left(1+\frac{\alpha x}{c^2}\right)\left(\frac{p^2}{2m_0} + m_0 c^2\right). \tag{11a}$$

In the classical level, the quantities H, x and p are treated as dynamical variables. Further, it can very easily be verified that in the quantum mechanical scenario where these quantities are considered to be operators, the Hamiltonian H is not hermitian. However the energy eigen spectrum for the Schrödinger equation has been observed to be real [10]. This is found to be solely because of the fact that H is PT-invariant. Now it is well know that $PxP^{-1} = -x$, $PpP^{-1} = -p$, whereas $TpT^{-1} = -p$ and $P\alpha P^{-1} = -\alpha$ but $T\alpha T^{-1} = \alpha$. Therefore, it is a matter of simple algebra to show that $PT\ H\ (PT)^{-1} = H^{PT} = H$. As has been shown by several authors [11] that if H is PT-invariant, then the energy eigen values will be real. Here P and T are respectively the parity and the time reversal operators. Further if the Hamiltonian is PT symmetric, then H and PT should have common eigen states. In [10] we have noticed that the solution of the Schrödinger equation is obtained in terms of the variable $u = 1 + \alpha x/c^2$, which is PT-symmetric. Hence any function, e.g., Whittaker function $M_{k,\mu}(u)$ or Associated Laguerre function $L_m^n(u)$, the solution of the Schrödinger equation are PT-symmetric. These polynomials are also the eigen functions of the operator PT.

Of course with the replacement of hermiticity of the Hamiltonian with the PT-symmetry, we have not discarded the important quantum mechanical key features of the system described by this Hamiltonian and also kept the canonical quantization rule invariant, i.e., $TiT^{-1} = -i$. This point was also discussed in an elaborate manner in reference [11] and in some of the references cited there.

In this article we have investigated the time evolution for both the space and the momentum coordinates of the particle moving in Rindler space. We have considered both the relativistic and the non-relativistic form of the Rindler Hamiltonian (Eqs. (11) and (11a) respectively). Hence we shall also obtain the classical phase space trajectories for the particle in the Rindler space. We have noticed that in the relativistic scenario, both the spatial and the momentum coordinates are real in nature and diverge as $t \longrightarrow \infty$. For both the variables the time dependencies are extremely simple. Hence we have obtained classical trajectories $p(x)$ by eliminating the time dependent part.

However, in the non-relativistic approximation, the spatial coordinates are quite complex in nature, whereas the momentum coordinates are purely imaginary. Since the mathematical form of the phase space trajectories are quite complicated, we have obtained $p(x)$ numerically in the non-relativistic scenario.

In the first part of this article, we have considered the relativistic picture and obtained the phase space trajectories, whereas in the second part, the classical phase space structure is obtained for non-relativistic case. To the best of our knowledge such studies have not been done before.

2. Relativistic Picture

The classical Hamilton's equation of motion for the particle is given by [12]

$$\dot{x} = [H, x]_{p.x} \quad \text{and} \quad \dot{p} = [H, p]_{p,x} \tag{12}$$

where $[H, f]_{p,x}$ is the Poisson bracket and is defined by [12]

$$[f, g]_{p,x} = \frac{\partial f}{\partial p}\frac{\partial g}{\partial x} - \frac{\partial f}{\partial x}\frac{\partial g}{\partial p}. \tag{13}$$

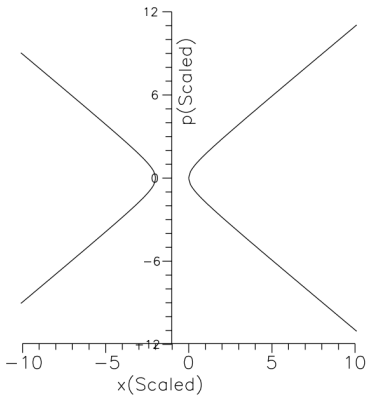

Fig. 1 Phase space trajectories for the relativistic scenario with the scaling parameters equal to unity

In this case $f = x$ or p. In Eq. (12) the dots indicate the derivative with respect to time. Now using the relativistic version of Rindler Hamiltonian from Eq. (11), the explicit form of the equations of motion are given by

$$\dot{x} = \left(1 + \frac{\alpha x}{c^2}\right) \frac{pc^2}{(p^2c^2 + m_0^2c^4)^{1/2}} \quad \text{and} \quad \dot{p} = -\frac{\alpha}{c}(p^2c^2 + m_0^2c^4)^{1/2}. \tag{14}$$

The parametric form of expressions for x and p represent the time evolution of spatial coordinate and the corresponding canonical momentum. The analytical expressions for time evolution for both the quantities can be obtained after integrating these coupled equations and are given by

$$x = \frac{c^2}{\alpha}[C_0 \cosh(\omega t - \phi) - 1] \quad \text{and} \quad p = -m_0 c \ \sinh(\omega t - \phi), \tag{15}$$

where C_0 and ϕ are the integration constants, which are real in nature and $\omega = \alpha/c$ is the frequency defined for some kind of quanta in [10]. Hence eliminating the time coordinate, we can write

$$\left(1 + \frac{\alpha x}{c^2}\right)^2 \frac{1}{C_0^2} - \frac{p^2}{m_0^2c^2} = 1. \tag{16}$$

This is the mathematical form of the set of classical trajectories of the particle in the phase space. Or in other wards, these set of hyperbolas are the classical trajectories of the particle in the Rindler space. This is consistent with the hyperbolic motion of the particle in a uniformly accelerated frame. These set of hyperbolic equations can also be written as

$$p^2 = m_0^2c^2 \left(\frac{2\alpha x}{c^2}\right)\left(1 + \frac{x\omega}{2c}\right). \tag{17}$$

It is quite obvious from the parametric form of the variation of x and p with time that both the quantities are unbound. This is also reflected from the nature of phase space trajectories as shown in Fig. 1 for the scaled x and p. The scaling

factors are α/c^2 for x and $(m_0c)^{-1}$ for p. For the sake of illustration, we have chosen the arbitrary constant $C_0 = 1$.

In this figure we have also taken both the scaling factors identically equal to unity. Then obviously Eq. (16) reduces to

$$(x+1)^2 - p^2 = 1.$$

We shall get the other set of trajectories by choosing different values for the scaling factors. It is obvious that in this case the centre of the hyperbola is at $(-1, 0)$. Therefore with the increase of α, the centre $\longrightarrow (0, 0)$. Further the vertices for this particular hyperbolic curve are at $(0, 0)$ and $(-2, 0)$. The second one is in scaled form. Therefore for the gravitational field α large enough, both the vertices coincide at the centre $(0, 0)$. It is also obvious that for very large values of α, these two curves touch each other at $(0, 0)$. We have therefore noticed that the phase space trajectories are unbound and consistent with the motion of the particle in Rindler space.

3. Non-Relativistic Picture

We next consider the non-relativistic form of Rindler Hamiltonian given by Eq. (11a). Now following Eq. (12), the equations of motion for the particle in Rindler space in the non-relativistic approximation are given by

$$\dot{x} = \left(1 + \frac{\alpha x}{c^2}\right)\frac{p}{m_0} \quad \text{and} \quad \dot{p} = -\frac{\alpha}{c^2}\left(\frac{p^2}{2m_0} + m_0c^2\right). \tag{18}$$

On integrating the second one we have

$$p = i2^{1/2}m_0c\cot\left(\frac{2^{1/2}\omega t + \phi}{2}\right) = ip_I. \tag{19}$$

The particle momentum is therefore purely imaginary in nature with its real part $p_R = 0$. Here ϕ is a real constant phase. Next evaluating the first integral analytically, we have

$$\begin{aligned} x = {} & \frac{c}{\omega}\left[-1 + \cos\left\{\ln\left(\sin^2\left(\frac{2^{1/2}\omega t - \phi}{2}\right)\right)\right\}\right] \\ & + i\frac{c}{\omega}\left[\sin\left\{\ln\left(\sin^2\left(\frac{2^{1/2}\omega t - \phi}{2}\right)\right)\right\}\right] = x_R + ix_I. \end{aligned} \tag{20}$$

The spatial part is therefore complex in nature, where the real part

$$x_R = \frac{c}{\omega}\left[-1 + \cos\left\{\ln\left(\sin^2\left(\frac{2^{1/2}\omega t - \phi}{2}\right)\right)\right\}\right] \tag{21}$$

and the corresponding imaginary part is given by

$$x_I = \frac{c}{\omega}\left[\sin\left\{\ln\left(\sin^2\left(\frac{2^{1/2}\omega t - \phi}{2}\right)\right)\right\}\right]. \tag{22}$$

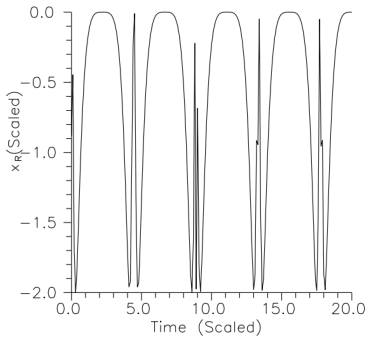

Fig. 2 Variation of scaled x_R with scaled time

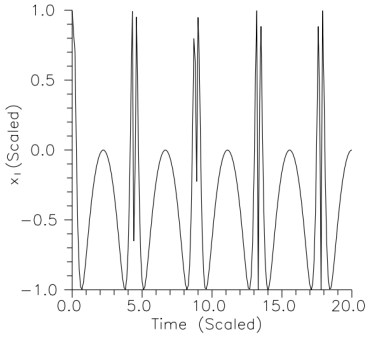

Fig. 3 Variation of scaled x_I with scaled time

Here again eliminating the time part, we have the mathematical form of phase space trajectories for the imaginary parts only

$$p_I = 2^{1/2} m_0 c \frac{\left[1 - \exp\left\{\sin^{-1}\left(\frac{\omega}{c} x_I\right)\right\}\right]^{1/2}}{\exp\left\{\frac{1}{2}\sin^{-1}\left(\frac{\omega}{c} x_I\right)\right\}}, \tag{23}$$

which gives the phase space trajectories of the particle in the Rindler space in non-relativistic scenario. It should be noted here that since the real part of the particle momentum is zero, we have considered the imaginary parts only. Since p_I is real, therefore $\mid \omega x_I/c \mid \leq 1$, i.e., can not have all possible values.

In Fig. 2 we have plotted the scaled x_R, i.e. $(\omega x_R/c)$ with scaled time $(\omega t/2^{1/2})$ for $\phi = 0$. Since the constant phase ϕ is completely arbitrary, for the sake of illustration we have chosen it to be zero. In this diagram the scaling factors are also taken to be unity. Now if we consider variation of the scaling factors, the qualitative nature of the graphs will not change but there will be quantitative changes.

In Fig. 3 we have plotted the scaled x_I, i.e., $(\omega x_I/c)$ with scaled time $(\omega t/2^{1/2})$ for $\phi = 0$. In this case also same type of changes as has been mentioned for x_R will be observed.

In Fig. 4 we have plotted the scaled p_I, which is actually $(p_I/2^{1/2} m_0 c)$ with scaled time $(\omega t/2^{1/2})$ for $\phi = 0$. In this case also the scaling factors are exactly

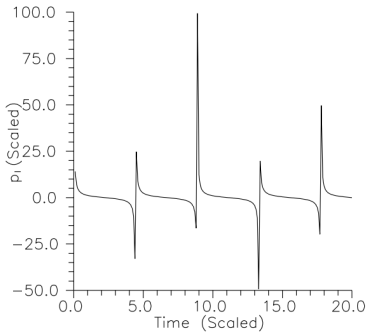

Fig. 4 Variation of scaled p_I with scaled time

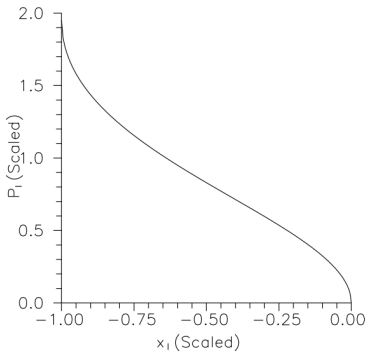

Fig. 5 Phase space trajectories for the non-relativistic scenario with the scaling parameters equal to unity

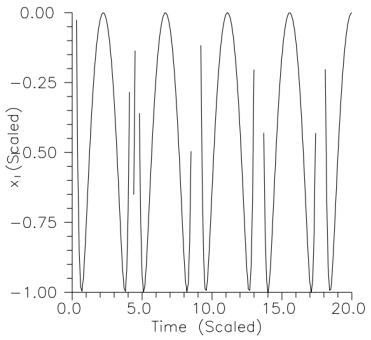

Fig. 6 Temporal variation of x_I in physically acceptable domain

equal to one. Further the same kind of variation as mentioned above will be observed for p_I with the change of scaling parameters.

Finally in Fig. 5 the phase space trajectory for scaled x_I and scaled p_I is shown Since the physically accepted domain for scaled x_I is from -1 to 0, we have shown in Figs. 6 and 7 the plot of scaled x_I and scaled p_I with scaled time.

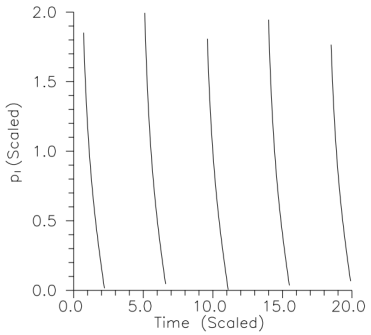

Fig. 7 Temporal variation of p_I in physically acceptable domain

4. Conclusion

Finally in conclusion we would like to mention that to the best of our knowledge this is the first time the phase space trajectories are obtained in Rindler space using non-hermitian PT-symmetric Hamiltonian.

In the relativistic case the trajectories can be represented by a set of hyperbolas. Whereas in the non-relativistic picture, particle momenta are purely imaginary and the space coordinates are complex in nature. The variation of real and imaginary parts of space coordinates are quite complicated. Further, the phase space is restricted within the domain of negative x-values. The imaginary part of particle momentum has been observed to change with time in a discrete manner in this region.

If we consider the Rindler Hamiltonian in the form

$$H = \left(1 + \frac{\alpha x}{c^2}\right) \frac{p^2}{2m} \tag{24}$$

then it is a matter of simple algebra to show that

$$1 + \frac{\omega x}{c} = t \exp(2m) \text{ and } p = \frac{2mc}{\omega t}. \tag{25}$$

Hence redefining $1+\omega x/c$ as new x and $2mc/(\omega p)\exp(2m)$ as new $1/p$, we have $xp = 1$, which gives the phase space trajectories in Rindler space. The trajectories are rectangular hyperbola.

References

1. L.D. Landau and E.M. Lifshitz, *The Classical Theory of Fields* (Butterworth-Heimenann, Oxford, 1975).
2. W.G. Rosser, *Contemporary Physics* **1** (1960) 453.
3. N.D. Birrell and P.C.W. Davies, *Quantum Field Theory in Curved Space* (Cambridge Univ. Press, Cambridge, 1982).
4. G.F. Torres del Castillo and C.L. Perez Sanchez, *Revista Mexican De Fisika* **52** (2006) 70.
5. M. Socolovsky, *Annales de la Foundation Louis de Broglie* **39** (2014) 1.
6. C.G. Huang and J.R. Sun, arXiv:gr-qc/0701078 (2007).
7. D.J. Louis-Martinez, *Class. Quantum Grav.* **28** (2011) 036004.

8. D. Percoco and V.M. Villaba, *Class. Quantum Grav.* **9** (1992) 307.
9. S. De, S. Ghosh and S. Chakrabarty, *Astrophys. Space Sci.*, DOI: 10.1007/s10509-015-2520-3.
10. S. De, S. Ghosh and S. Chakrabarty, *Mod. Phys. Lett. A* **30** (2015) 1550182.
11. C.M. Bender, arXiv:quant-ph/0501052 (and references therein).
12. H. Goldstein, *Classical Mechanics* (Addision Wesley, 1972).

Scientific Voyage
Vol. 2, No. 1,
Page 20-28 (2021)

SCIENTIFIC VOYAGE
ISSN: 2395-5546

GCECT
Publication
Jan.-Mar.

Modified Newtonian Gravity: Explaining observations of sub- and super-Chandrasekhar limiting mass white dwarfs

Agrim Sharma[1] and Banibrata Mukhopadhyay[2]
Department of Physics, Indian Institute of Science, Bangalore 560012, India

Abstract: The idea of possible modification to gravity theory, whether it is in the Newtonian or general relativistic premises, is there for quite sometime. Based on it, astrophysical and cosmological problems are targeted to solve. But none of the Newtonian theories of modification has been performed from the first principle. Here, we modify Poisson's equation and propose two possible ways to modify the law gravitation which, however, reduces to Newton's law far away from the center of source. Based on these modified Newton's laws, we attempt to solve problems lying with white dwarfs. There are observational evidences for possible violation of the Chandrasekhar mass-limit significantly: it could be sub- as well as super-Chandrasekhar. We show that modified Newton's law, either by modifying LHS or RHS of Poisson's equation, can explain them.

Keywords: Newton's law; modified Poisson's equation; Chandrasekhar-limit; white dwarf

1. Introduction

Over the years, the researchers have explored the modifications to Einstein's gravity in order to explain astrophysical and cosmological data. However, any such modification proposed for the compact objects should be asymptotically flat. It should follow the reduction from modified Einstein's to Einstein's gravities and then to Newtonian gravity with distance from the source. Therefore, a modified Einstein's gravity may reduce to modified Newtonian gravity at some length scale.

In the present paper, we explore the possible modification to Poisson's equation to understand the possible modification to Newtonian gravity. Based on that, we target to resolve an astrophysical problem.

A white dwarf is a stellar core remnant composed mostly of electron-degenerate matter. The Chandrasekhar-limit is a theoretical limit for the maximum mass of a stable nonrotating and nonmagnetized white dwarf. If the mass of a white dwarf exceeds this limit, the force due to gravity becomes greater than that due to the electron degeneracy pressure. This leads to the star collapsing under its own gravity, leading to heating up of the plasma, which can result in a supernova. This is what happens in a type Ia supernova (SNIa).

A typical, slowly rotating, carbon-oxygen white dwarf accreting mass from a companion star explodes at a critical mass $\sim 1.4M_{\odot}$. Due to this, all type Ia supernovae (SNeIa) have a characteristic light curve, that is luminosity as a function of time. This makes SNeIa a "standard candle", which can be used to study the universe in various ways. Notably, observations of SNeIa led to the conclusion that the universe is undergoing an accelerated expansion.

[1] E-mail: agrimsharma@iisc.ac.in
[2] E-mail: bm@iisc.ac.in

However, there are observations of highly over-luminous SNeIa, e.g., SN 2003fg, SN 2006gz, SN 2007if, SN 2009dc [1,2] with progenitor masses believed to be as high as $2.8 M_{\odot}$ and highly under-luminous SNeIa, e.g., SN 1991bg, SN 1997cn, SN 1998de, SN 1999by, SN 2005bl with inferred progenitor masses being as low as $0.5\ M_{\odot}$ [3–5].

As a possible explanation of these anomalous SNeIa, Mukhopadhyay and his collaborators had earlier explored modifications to general relativistic gravity models and the resulting change in the Chandrasekhar mass-limit [6,7].

This work explores similar modifications to Newton's model of gravity to see if modifications to corresponding classical quantities also produce similar results.

2. The Modification to Newtonian gravity

The aim here is to have a formula that is able to reproduce Newtonian results in the weak field limit and mimic general relativistic results in the strong field limit. The original Poisson's equation for Newtonian gravitational potential $\phi(\mathbf{r})$ for a density distribution $\rho(\mathbf{r})$ is

$$\nabla^2\phi = 4\pi\rho G. \tag{1}$$

The following are two general types of modifications that are considered in this work:

$$\nabla^2\phi + A\nabla^4\phi = 4\pi\rho G \tag{2}$$

$$\nabla^2\phi = 4\pi G(\rho + B\rho^2 + ...). \tag{3}$$

3. LHS modification: general solution to the equation

The modified formula can be provided as

$$\nabla^2\phi + A\nabla^4\phi = 4\pi\rho G. \tag{4}$$

Using Green's method, with the constraint that $\phi \in \mathbb{R}$, we get the following expressions:

$$\text{For } A>0\text{: } \phi(\mathbf{r}) = \int \frac{d^3\mathbf{r'}}{4\pi|\mathbf{r}-\mathbf{r'}|}\left(\int d^3\mathbf{r''}\frac{\cos\left(\frac{|\mathbf{r'}-\mathbf{r''}|}{A}\right)}{4\pi|\mathbf{r'}-\mathbf{r''}|}\frac{4\pi G\rho(\mathbf{r''})}{A}\right), \tag{5}$$

$$\text{For } A<0\text{:}\phi(\mathbf{r}) = \int \frac{d^3\mathbf{r'}}{4\pi|\mathbf{r}-\mathbf{r'}|}\left(\int d^3\mathbf{r''}\frac{\exp\left(-\frac{|\mathbf{r'}-\mathbf{r''}|}{\sqrt{|A|}}\right)}{4\pi|\mathbf{r'}-\mathbf{r''}|}\frac{4\pi G\rho(\mathbf{r''})}{|A|}\right). \tag{6}$$

We have provided detailed explanation in Appendix A.

3.1 Calculation of the mass limit

Coming to the ideal white dwarf model which satisfies the equations:

$$P = K\rho^{1+\frac{1}{n}}, \tag{7}$$

$$\frac{dM_r}{dr} = 4\pi r^2 \rho, \tag{8}$$

$$\frac{\nabla P}{\rho} = -\nabla\phi, \tag{9}$$

$$\implies \frac{1}{r^2}\frac{d}{dr}\left(\frac{r^2}{\rho}\frac{dP}{dr}\right) = -\nabla^2\phi = -f(r), \tag{10}$$

where P is the pressure of white dwarf matter, ρ the density, M_r the mass enclosed in the radius r, n the polytropic index and K the polytropic constant.

Let θ be a dimensionless function of r so that

$$\rho(r) \equiv \rho = \rho_c \theta^n, \tag{11}$$

where ρ_c being the density at the centre of the white dwarf.

Similarly, considering dimensionless variable ξ such that

$$r = a\xi, \tag{12}$$

we obtain

$$-f(r) = \frac{1}{r^2}\frac{d}{dr}\left(\frac{r^2}{\rho}\frac{dP}{dr}\right) = \frac{(1+n)K\rho_c^{1/n}}{a^2}\frac{1}{\xi^2}\frac{d}{d\xi}\left(\xi^2\frac{d\theta}{d\xi}\right). \tag{13}$$

From the modified equation for gravity given by Eq. (4):

$$f(r) + A\frac{1}{r^2}\frac{d}{dr}\left(r^2\frac{df}{dr}\right) = g(r) = 4\pi\rho_c\theta^n G, \tag{14}$$

$$\left(\frac{2}{\xi}\frac{d\theta}{d\xi} + \frac{d^2\theta}{d\xi^2}\right) + \frac{A}{a^2}\left(\frac{4}{\xi}\frac{d^3\theta}{d\xi^3} + \frac{d^4\theta}{d\xi^4}\right) = -\frac{a^2 4\pi G}{(1+n)K\rho_c^{\frac{1-n}{n}}}\theta^n. \tag{15}$$

If we let $a^2 = \frac{(1+n)K\rho_c^{\frac{1-n}{n}}}{4\pi G}$, then we obtain

$$\left(\frac{2}{\xi}\frac{d\theta}{d\xi} + \frac{d^2\theta}{d\xi^2}\right) + \frac{A}{a^2}\left(\frac{4}{\xi}\frac{d^3\theta}{d\xi^3} + \frac{d^4\theta}{d\xi^4}\right) = -\theta^n. \tag{16}$$

Notice that when $A = 0$, the above equation reduces to the Lane-Emden equation as expected.

For $n = 3$ (i.e. the relativistic case), we will numerically find the solution of $\theta(\xi)$, which will give us the mass-limit of a white dwarf as a function of A/a^2 based on

$$M = \int_0^R 4\pi r^2 \rho dr = 4\pi a^3 \rho_c \int_0^{\xi_1} \xi^2 \theta^n d\xi. \tag{17}$$

3.2 Numerical solution of $\rho(r)$ for white dwarfs

Having added a new parameter to the Lane-Emden equations, we will need some extra information than what is usually needed to find numerical solutions in the Newtonian gravity. Fig. 1 shows the variation of M_{lim}/M_{Ch}, with M_{lim} being new mass-limit and M_{Ch} being original Chandrasekhar-limit, as a function of a^2/A for different values of the extra unknown constraint $\theta''(0)$ shown as labels.

Since 'a' depends on ρ_c and n, we can obtain different values of Chandrasekhar-limit for different ρ_c and even subtly different n, both of which are physical parameters. Hence given a fixed value of the modification parameter A which we naturally expect to be a universal constant, there can be conditions where the Chandrasekhar mass-limit differs depending on conditions inside the white dwarf.

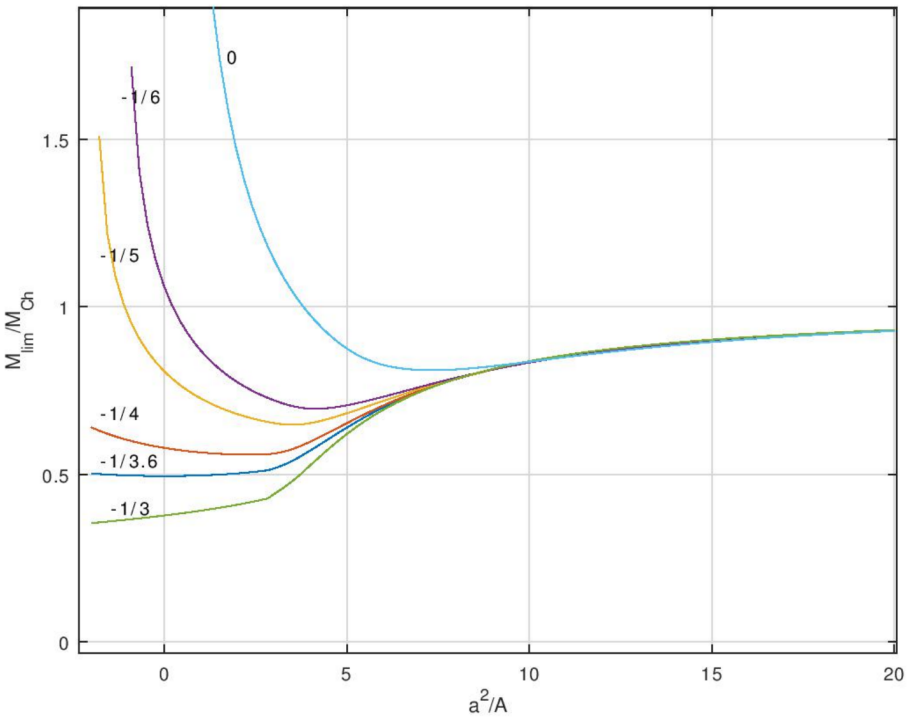

Fig. 1 Variation of M_{lim}/M_{Ch} with a^2/A for different $\theta''(0)$ shown as labels.

3.3 Analytical limits of M_{lim}/M_{Ch} as $A \to 0$ and $A \to \infty$

The modified Lane-Emden equation is

$$\left(\frac{2}{\xi}\frac{d\theta}{d\xi} + \frac{d^2\theta}{d\xi^2}\right) + \frac{A}{a^2}\left(\frac{4}{\xi}\frac{d^3\theta}{d\xi^3} + \frac{d^4\theta}{d\xi^4}\right) = -\theta^n. \tag{18}$$

Analytical limits can give us some verification of the correctness of numerical solutions. For example, the results in Fig. 1 appear to be correct at least in the $a^2/A \geq 0$ regime.

3.3.1 Limit $A \to 0$:

For $A/a^2 << 1$, assuming slight perturbation to the original Lane-Emden equation, the solution gives us:

$$\frac{M_{lim}}{M_{Ch}} = \frac{\int_0^{\xi_1} \xi^2 \theta^3 d\xi}{2.01824} = \left(1 + \frac{A}{a^2}\frac{2.1173}{2.01824}\right)\left(1 - 3\frac{A}{a^2}\right). \tag{19}$$

Fig. 2 confirms that the solution passes $A = 0$ point smoothly with $M_{lim}/M_{Ch} = 1$, confirming the correctness of results around $A = 0$.

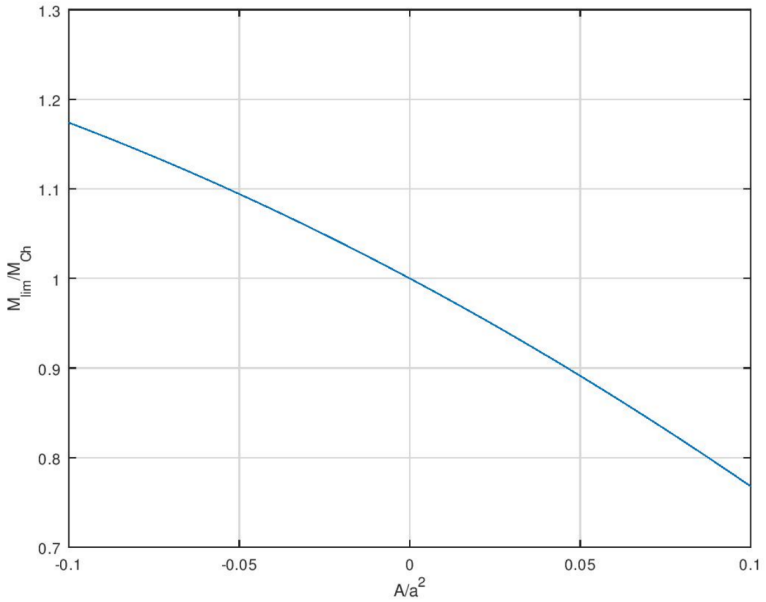

Fig. 2 Variation of M_{lim}/M_{Ch} with A/a^2 around $A = 0$.

3.3.2 Limit $A \to \infty$:

In this case the mass-limit depends on second derivative of $\theta(r) = [\rho(r)/\rho(0)]^{1/n}$ (where $\rho(0) = \rho_c$) at the centre of the white dwarf, and hence we obtain

$$\frac{M_{lim}}{M_{Ch}} = \frac{1}{15}\left(\frac{-2}{\theta''(0)}\right)^{3/2}. \tag{20}$$

3.4 Mass-radius relation

For the mass-radius relation, the density as a function of distance from center is numerically computed[3] using the following equations:

$$\frac{dM_r}{dr} = 4\pi r^2 \rho, \tag{21}$$

$$\frac{\nabla P}{\rho} = -\nabla \phi. \tag{22}$$

Chandrasekhar's exact equation of state is given by

$$P = K_1 \left[x(2x^2 - 3)\sqrt{x^2+1} + 3\sinh^{-1} x \right], \tag{23}$$

$$\rho = K_2 x^3, \tag{24}$$

where $K_1 = 8\pi\mu_e m_H (m_e c)^3/3h^3$ and $K_2 = \pi m_e^4 c^5/3h^3$.

The modified gravity equation is:

$$\nabla^2\phi + A\nabla^4\phi = 4\pi\rho G. \tag{25}$$

Fig. 3 shows the variation radius of white dwarfs as a function of their mass.

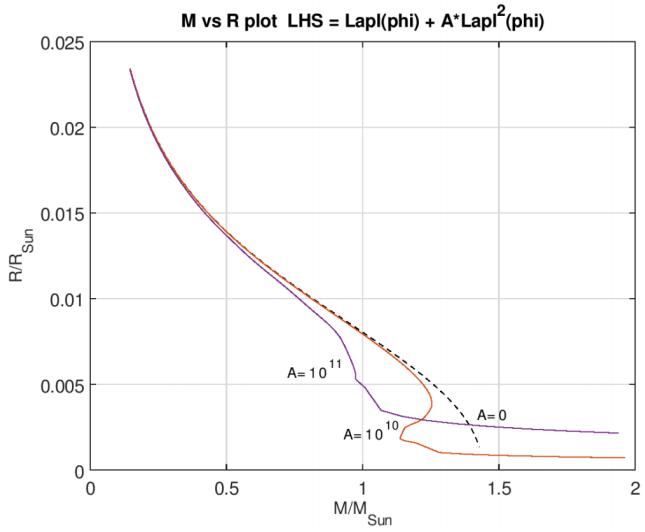

Fig. 3 Variation of radius with mass, where A is in units of m^2. The central density varies from $\rho_c = 10^8$ to $10^{13} kg/m^3$.

[3] Using GNU Octave's 'ode15s' function - a variable step, variable order method based on Backward Difference Formulas (BDF).

4. RHS modification: general solution to the equation

The modified formula in this case is

$$\nabla^2\phi = 4\pi G(\rho + B\rho^2 + ...). \tag{26}$$

Let $\rho_{\text{eff}} = \rho + B\rho^2 + ...$

We explicitly know the solution of the Poisson equation $\nabla^2\phi = \rho_{\text{eff}}(\mathbf{r})$ is

$$\phi(\mathbf{r}) = -\int \frac{\rho_{\text{eff}}(\mathbf{r'})}{4\pi|\mathbf{r}-\mathbf{r'}|} d^3\mathbf{r'}. \tag{27}$$

Therefore, the form of gravitational potential will be exactly same as the usual Newtonian gravitational potentials, but with ρ_{eff} instead of ρ.

4.1 Mass-radius relation

Using the same method as in Sec. 3, with the new modified gravity equation, the variation of radius for white dwarfs as a function of their mass is generated numerically[4].

The modified equation considered is

$$\nabla^2\phi = 4\pi G(\rho + A\rho^2). \tag{28}$$

One can observe in Fig. 4 that when $\rho_{\text{eff}} > \rho$, the mass is lower for a given radius, as expected, and likewise for $\rho_{\text{eff}} < \rho$, the mass is higher than usual white dwarf mass, obtained based on Newton's law, for the same radius. Therefore, using higher order polynomial terms, at different densities, the white dwarf can show arbitrarily small or large masses in the range of ρ where the respective terms dominate.

5. Conclusion

Newton's law is a remarkably successful physics, well tested in laboratory, also is remarkably successful in explaining low energy physics. Several astrophysical features are also quite abide it. In this connection, the Chandrasekhar-limit perhaps is one of the most celebrated astrophysical discoveries in the 20th century, whose physical insight can be well understood in the Newtonian framework itself. However, observations of several peculiar over- and under-luminous SNeIa for about last three decades argue for the significant violation of the Chandrasekhar mass-limit. We have shown here that appropriate modifications to Poisson's equation and, hence, Newton's law can explain the significant violation of the Chandrasekhar-limit, as inferred from observations. It argues that while the existence of the Chandrasekhar-limit is sacrosanct, its value need not be. We expect the proposed modifications to Poisson's equation and modified Newton's law, which reduces to Newton's law asymptotically, to have far reaching implications.

[4] Using GNU Octave's 'ode15s' function - a variable step, variable order method based on Backward Difference Formulas (BDF).

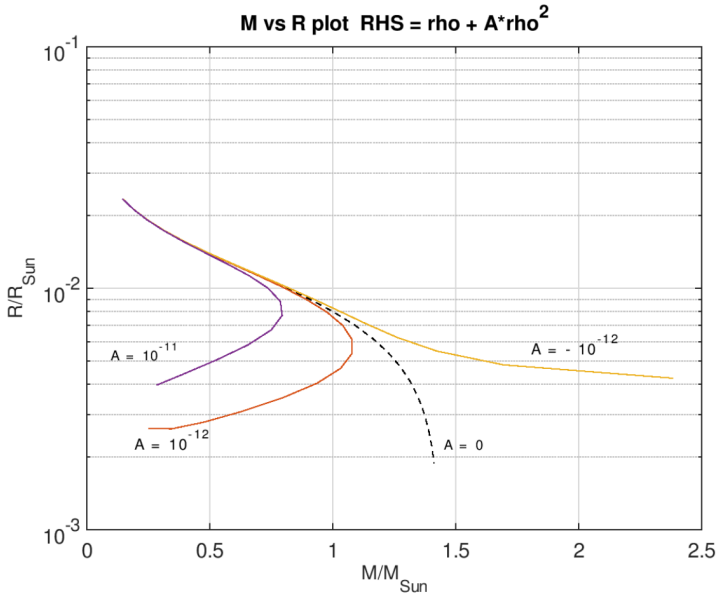

Fig. 4 Variation of radius with mass, where A is in units of m^3/kg. The central density varies from $\rho_c = 10^8$ to $10^{11} kg/m^3$.

Appendix A: General solution of the equation with modified LHS

The modified equation is given by

$$\nabla^2\phi + A\nabla^4\phi = 4\pi\rho G. \tag{29}$$

$$\text{Let } u(\mathbf{r}) = \nabla^2\phi(\mathbf{r}),$$

$$\implies \left[A\nabla^2 + 1\right] u(\mathbf{r}) = 4\pi\rho G. \tag{30}$$

From the solution of Screened Poisson Equation (derived using Green's functions)

$$\left[\nabla^2 - \lambda^2\right] u(\mathbf{r}) = -f(\mathbf{r}), \tag{31}$$

$$\implies u(\mathbf{r}) = \int d^3\mathbf{r'} \frac{e^{-\sqrt{\lambda^2}|\mathbf{r}-\mathbf{r'}|}}{4\pi|\mathbf{r}-\mathbf{r'}|} f(\mathbf{r'}). \tag{32}$$

For $A < 0$, $\quad \lambda^2 = \frac{1}{|A|}, f = \frac{4\pi\rho G}{|A|},$

$$u(r \to \infty) \to 0 \implies \lambda = \frac{1}{\sqrt{|A|}}.$$

Hence

$$u(\mathbf{r}) = \nabla^2\phi(\mathbf{r}) \implies \phi(\mathbf{r}) = \int \frac{d^3\mathbf{r'}}{4\pi|\mathbf{r}-\mathbf{r'}|} u(\mathbf{r'}), \tag{33}$$

$$\phi(\mathbf{r}) = \int \frac{d^3\mathbf{r'}}{4\pi|\mathbf{r}-\mathbf{r'}|}\left(\int d^3\mathbf{r''}\frac{\exp\left(-\frac{|\mathbf{r'}-\mathbf{r''}|}{\sqrt{|A|}}\right)}{4\pi|\mathbf{r'}-\mathbf{r''}|}\frac{4\pi G\rho(\mathbf{r''})}{|A|}\right). \tag{34}$$

Similarly, for $A > 0$, $\lambda^2 = -\frac{1}{A}, f = -\frac{4\pi\rho G}{A}$,

$$u(r) \in \mathbb{R} \implies e^{-\lambda|\mathbf{r}-\mathbf{r'}|} \equiv \frac{1}{2}\left(e^{\frac{-\iota}{\sqrt{A}}|\mathbf{r}-\mathbf{r'}|} + e^{\frac{\iota}{\sqrt{A}}|\mathbf{r}-\mathbf{r'}|}\right) \equiv \cos\left(\frac{1}{\sqrt{A}}|\mathbf{r}-\mathbf{r'}|\right).$$

Therefore

$$\phi(\mathbf{r}) = \int \frac{d^3\mathbf{r'}}{4\pi|\mathbf{r}-\mathbf{r'}|}\left(\int d^3\mathbf{r''}\frac{\cos\left(\frac{|\mathbf{r'}-\mathbf{r''}|}{A}\right)}{4\pi|\mathbf{r'}-\mathbf{r''}|}\frac{4\pi G\rho(\mathbf{r''})}{A}\right). \tag{35}$$

References

1. D.A. Howell et al., *Nature* **443** (2006) 308.
2. R.A. Scalzo et al., *ApJ* **713** (2010) 1073.
3. A.V. Filippenko et al., *AJ* **104** (1992) 1543.
4. P.A. Mazzali et al., *Mon. Not. R. Astron. Soc.* **284** (1997) 151.
5. S. González-Gaitán et al., *ApJ* **727** (2011) 107.
6. U. Das and B. Mukhopadhyay, *JCAP* **5** (2015) 045.
7. S. Kalita and B. Mukhopadhyay, *JCAP* **9** (2018) 007.

Scientific Voyage
Vol. 2, No. 1,
Page 29-38 (2021)

SCIENTIFIC VOYAGE
ISSN: 2395-5546

GCECT
Publication
Jan.-Mar.

Coherent propagation dynamics of an adiabatic four-waveguide directional coupler: a generic approach

Indranil Bayal[a] and Pradipta Panchadhyayee[1,b]

[a] *Gopinathpur High School, Gopinathpur, Purba Medinipur, W.B., 72 1633, India*

[b] *Department of Physics, P. K. College, Contai, Purba Medinipur, W.B., 72 1401, India*

Abstract. A generic model is presented to explore optical analogues of coherent population transfer and trapping in a four-waveguide (WG) directional coupler. In contrast to conventional counterintuitive order for the coupling coefficients, the present model highlights the robustness of the approach irrespective of any particular coupling order with varying conditions of initial light distribution. The coherent propagation characteristics shown by the WG coupler involve all the adiabatic states instead of dark states only.

Keywords: Coherent population transfer and trapping, four-waveguide directional coupler, tripod system, adiabatic states.

1. Introduction

During past few decades, some researchers have focused their attention to investigate the probability of exploration of the microscopic quantum phenomena in optical regime. It provides ample advantage of directly mapping the evolution of wave function in space by simple fluorescence imaging or scanning tunneling optical microscopy. The field opto-quantum analogy has become interesting day by day opening up a new avenue with the emergence of coherent laser source and integrated fiber optics. The opto-quantum analogy have been extended to the field of quantum optics to emulate many interesting phenomena like strongly driven two-level system and Rabi oscillations, Electromagnetically Induced Transparency, Fano Interference, Stabilization of Atoms in Ultra Strong Laser Fields, Stimulated Raman Adiabatic Passage (STIRAP)linked with Coherent Population Trapping (CPT), quantum state embedded in a continuum accompanied by Fano Resonance, quantum information processing and quantum teleportation in photonic structures. WG based photonic structures are frequently used in this quest since optical analogue of laser-matter interaction effects can be effortlessly produced by simple engineering of the guiding structure [1,2]. The direct mapping and space visualization of ultrafast time dependent phenomena is feasible using coupled WG and fiber structure. WG array and directional coupler have been proven to be important optical tools for reproducing microscopic quantum phenomena. WG array based photonic configurations are also employed to

[1] **Corresponding Author:** ppcontai@gmail.com

investigate quantum phenomena like Coherent Population Transfer [3-6] and Trapping [7,8], Fano Resonance [7], Rabi Oscillation [9] effects in broader scale.

In guided wave communication systems, optical WG directional couplers have promising potential applications including power splitting, switching etc. [10-13]. In the simplest form, directional couplers consist of two WGs which are installed sufficiently close so as to allow a coupling between them. As a result, the interference between the two modal fields leads to the periodical exchange of light energy between the two WGs during propagation [14]. Three or more evanescently coupled WG systems have attracted great research interest towards investigation of sophisticated and intriguing behavior in the field dynamics. The schemes for using three-WG couplers have been introduced by Iwasaki *et al.* [15] and experimentally demonstrated by Peall and Syms [16]. The extensive use of the directional coupler as a switching/modulating device has been theoretically and experimentally shown in various configurations and materials. The switching characteristics are analyzed in the three-WG system by launching an incident beam into either the central WG [17] or an outer WG [18,19] or in both [20,21]. The switching of light is feasible with the adiabatic evolution and the suitable design of variable coupling coefficients [19] *viz.* introducing the counterintuitive order. The adiabatic method is expedient as it needs no specific shape of coupling coefficient or definite system parameters. However, to ensure the adiabatic evolution of normal modes, the coupling profiles must allow sufficient overlapping over a significant spatial extent.

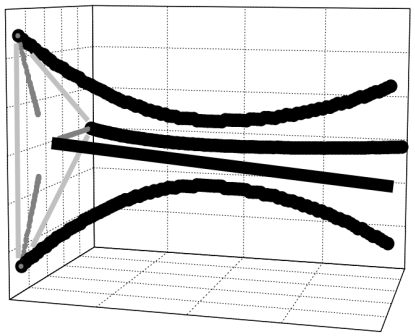

Fig. 1: Schematic presentation of a four-WG directional coupler.

Recently, an adiabatic three-WG coupler is presented in which the initial light is launched in each of the WGs and any sequence of coupling profiles can be allowed to employ [22]. Apart from switching and power splitting, WG directional couplers find applications as self-trapper (complete return of light to the initial state) too [23]. Coherent Population Transfer and CPT in multi-level atomic systems may be envisioned as the quantum analogues of switching, power splitting and self-trapping effects in coupler systems. In most of the previous works on directional couplers, the numbers of WGs were restricted to three only. In our present article, we study the adiabatic light transfer mechanism (optical analogue of coherent population transfer and trapping) in a four-WG directional coupler which assumes tripod like configuration in

atomic regime. In almost all earlier works counterintuitive coupling schemes have been used whereas our present study involves any order of coupling schemes and thereby making our approach more general. Also the initial light distribution condition can be varied arbitrarily.

2. Theory and Results

Adiabatic four-WG coupler analogous to a four-level tripod system is presented in Fig.1. In our configuration WG1, WG2 and WG3 are placed to make a small array and the rest WG4 is side coupled with WG2. The coupling coefficients between: WG1 and WG2 is $k_{12}(z)$, WG2 and WG3 is $k_{23}(z)$, WG2 and WG4 is $k_{24}(z)$ whereas coupling between other pairs of WGs have been ignored. We further assume that the propagation constants of all the WGs are equal. In resonant condition, the tripod like four WG system is described by the Hamiltonian

$$H(z)=\hbar\begin{pmatrix} 0 & k_{12} & 0 & 0 \\ k_{12} & 0 & k_{23} & k_{24} \\ 0 & k_{23} & 0 & 0 \\ 0 & k_{24} & 0 & 0 \end{pmatrix} \tag{1}$$

where coupling terms are real and satisfy the relation, $k_{ij}=k_{ji}$. Hamiltonian (represented by Eq. (1)) has four eigen values (two of which are equal) given by $\lambda_1=\lambda_2=0$, $\lambda_3=-\lambda_4=\hbar k(z)$ and $k(z)=\left(k_{12}^2+k_{23}^2+k_{24}^2\right)^{1/2}$. The corresponding adiabatic states can be expressed in terms of two z dependent mixing angles defined as $\tan\vartheta(z)=\dfrac{k_{12}(z)}{\left(k_{23}^2(z)+k_{24}^2(z)\right)^{1/2}}$ and $\tan\varphi(z)=\dfrac{k_{24}(z)}{k_{23}(z)}$.

The adiabatic states corresponding to two zero eigen values (dark states) are

$$\phi_1(z)=\psi_1\cos\vartheta(z)-\psi_3\sin\vartheta(z)\cos\varphi(z)-\psi_4\sin\vartheta(z)\sin\varphi(z) \tag{2}$$

$$\phi_2(z)=\psi_3\sin\varphi(z)-\psi_4\cos\varphi(z). \tag{3}$$

Two remaining adiabatic states are

$$\phi_3(z)=\frac{1}{\sqrt{2}}\left[\psi_1\sin\vartheta(z)+\psi_2+\psi_3\cos\vartheta(z)\cos\varphi(z)+\psi_4\cos\vartheta(z)\sin\varphi(z)\right] \quad (4)$$

$$\phi_4(z)=\frac{1}{\sqrt{2}}\left[\psi_1\sin\vartheta(z)-\psi_2+\psi_3\cos\vartheta(z)\cos\varphi(z)+\psi_4\cos\vartheta(z)\sin\varphi(z)\right] \quad (5)$$

in this regard an interesting point to highlight is that our four WG system is capable of generating double dark resonance. The amplitudes in the original and adiabatic bases are linked through the relation $\phi(z)=M(z)\psi(z)$ where the propagation matrix $M(z)$ is orthogonal and assumes the form

$$M(z)=\begin{pmatrix} \cos\vartheta & 0 & -\sin\vartheta\cos\varphi & -\sin\vartheta\sin\varphi \\ 0 & 0 & \sin\varphi & -\cos\varphi \\ \frac{1}{\sqrt{2}}\sin\vartheta & \frac{1}{\sqrt{2}} & \frac{1}{\sqrt{2}}\cos\vartheta\cos\varphi & \frac{1}{\sqrt{2}}\cos\vartheta\sin\varphi \\ \frac{1}{\sqrt{2}}\sin\vartheta & -\frac{1}{\sqrt{2}} & \frac{1}{\sqrt{2}}\cos\vartheta\cos\varphi & \frac{1}{\sqrt{2}}\cos\vartheta\sin\varphi \end{pmatrix} \quad (6)$$

The evolution matrix $U^A(z_f,z_i)$ in the adiabatic basis relates initial and final states such that $\phi(z_f)=U^A(z_f,z_i)\phi(z_i)$ where z_i and z_f represent the input and output z coordinates respectively. The evolution matrix in original basis reads as

$$U(z_f,z_i)=M^{-1}(z_f)U^A(z_f,z_i)M(z_i) \quad (7)$$

where

$U^A(z_f,z_i)=\begin{pmatrix} e^{i\eta_1} & 0 & 0 & 0 \\ 0 & e^{i\eta_2} & 0 & 0 \\ 0 & 0 & e^{i\eta_3} & 0 \\ 0 & 0 & 0 & e^{i\eta_4} \end{pmatrix}$ contains the phase factors in its diagonal elements.

The different elements of the evolution matrix can be explicitly written as:

$$U_{11}=\cos\vartheta_f\cos\vartheta_i e^{i\eta_1}+\frac{1}{2}\sin\vartheta_f\sin\vartheta_i e^{i\eta_3}+\frac{1}{2}\sin\vartheta_f\sin\vartheta_i e^{i\eta_4}$$

$$U_{12}=\frac{1}{2}\sin\vartheta_f e^{i\eta_3}-\frac{1}{2}\sin\vartheta_f e^{i\eta_4}$$

$$U_{13} = -\cos\vartheta_f \sin\vartheta_i \cos\varphi_i e^{i\eta_1} + \frac{1}{2}\sin\vartheta_f \cos\vartheta_i \cos\varphi_i e^{i\eta_3} + \frac{1}{2}\sin\vartheta_f \cos\vartheta_i \cos\varphi_i e^{i\eta_4}$$

$$U_{14} = -\cos\vartheta_f \sin\vartheta_i \sin\varphi_i e^{i\eta_1} + \frac{1}{2}\sin\vartheta_f \cos\vartheta_i \sin\varphi_i e^{i\eta_3} + \frac{1}{2}\sin\vartheta_f \cos\vartheta_i \sin\varphi_i e^{i\eta_4}$$

$$U_{21} = \frac{1}{2}\sin\vartheta_i e^{i\eta_3} - \frac{1}{2}\sin\vartheta_i e^{i\eta_4}$$

$$U_{22} = \frac{1}{2}e^{i\eta_3} + \frac{1}{2}e^{i\eta_4}$$

$$U_{23} = \frac{1}{2}\cos\vartheta_i \cos\varphi_i e^{i\eta_3} - \frac{1}{2}\cos\vartheta_i \cos\varphi_i e^{i\eta_4}$$

$$U_{24} = \frac{1}{2}\cos\vartheta_i \sin\varphi_i e^{i\eta_3} - \frac{1}{2}\cos\vartheta_i \sin\varphi_i e^{i\eta_4}$$

$$U_{31} = -\cos\vartheta_i \sin\vartheta_f \cos\varphi_f e^{i\eta_1} + \frac{1}{2}\sin\vartheta_i \cos\vartheta_f \cos\varphi_f e^{i\eta_3} + \frac{1}{2}\sin\vartheta_i \cos\vartheta_f \cos\varphi_f e^{i\eta_4}$$

$$U_{32} = \frac{1}{2}\cos\vartheta_f \cos\varphi_f e^{i\eta_3} - \frac{1}{2}\cos\vartheta_f \cos\varphi_f e^{i\eta_4}$$

$$U_{33} = \sin\vartheta_f \cos\varphi_f \sin\vartheta_i \cos\varphi_i e^{i\eta_1} + \sin\varphi_f \sin\varphi_i e^{i\eta_2} + \frac{1}{2}\cos\vartheta_f \cos\varphi_f \cos\vartheta_i \cos\varphi_i e^{i\eta_3}$$

$$+\frac{1}{2}\cos\vartheta_f \cos\varphi_f \cos\vartheta_i \cos\varphi_i e^{i\eta_4}$$

$$U_{34} = \sin\vartheta_f \cos\varphi_f \sin\vartheta_i \sin\varphi_i e^{i\eta_1} - \sin\varphi_f \cos\varphi_i e^{i\eta_2} + \frac{1}{2}\cos\vartheta_f \cos\varphi_f \cos\vartheta_i \sin\varphi_i e^{i\eta_3}$$

$$+\frac{1}{2}\cos\vartheta_f \cos\varphi_f \cos\vartheta_i \sin\varphi_i e^{i\eta_4}$$

$$U_{41} = -\cos\vartheta_i \sin\vartheta_f \sin\varphi_f e^{i\eta_1} + \frac{1}{2}\sin\vartheta_i \cos\vartheta_f \sin\varphi_f e^{i\eta_3} + \frac{1}{2}\sin\vartheta_i \cos\vartheta_f \sin\varphi_f e^{i\eta_4}$$

$$U_{42} = \frac{1}{2}\cos\vartheta_f \sin\varphi_f e^{i\eta_3} - \frac{1}{2}\cos\vartheta_f \sin\varphi_f e^{i\eta_4}$$

$$U_{43} = \sin\vartheta_i \cos\varphi_i \sin\vartheta_f \sin\varphi_f e^{i\eta_1} - \sin\varphi_i \cos\varphi_f e^{i\eta_2} + \frac{1}{2}\cos\vartheta_i \cos\varphi_i \cos\vartheta_f \sin\varphi_f e^{i\eta_3}$$

$$+\frac{1}{2}\cos\vartheta_i\cos\varphi_i\cos\vartheta_f\sin\varphi_f e^{i\eta_4}$$

$$U_{44}=\sin\vartheta_f\sin\varphi_f\sin\vartheta_i\sin\varphi_i e^{i\eta_1}+\cos\varphi_f\cos\varphi_i e^{i\eta_2}+\frac{1}{2}\cos\vartheta_f\sin\varphi_f\cos\vartheta_i\sin\varphi_i e^{i\eta_3}$$

$$+\frac{1}{2}\cos\vartheta_f\sin\varphi_f\cos\vartheta_i\sin\varphi_i e^{i\eta_4}$$

Let us assume $z_i=-\infty$ and $z_f=+\infty$

2.1 We now consider four distinct cases of coupling arrangements:

2.1.1 Case 1

The coupling coefficients are arranged in a manner such that $k_{23}(z)$ originates before and terminates after $k_{12}(z)$ whereas $k_{24}(z)$ is delayed with respect to both $k_{23}(z)$ and $k_{12}(z)$. Following Asymptotic relations are applicable for the aforementioned coupling sequence: $\vartheta_i(z=-\infty)=\vartheta_f(z=+\infty)=\phi_i(z=-\infty)=0,\phi_f(z=+\infty)=\frac{\pi}{2}$.Considering such arrangement we take four different cases of initial light distributions.

(i) If the initial amplitude is given by the matrix $(1,0,0,0)^T$, the final light amplitude will be $(e^{i\eta_1},0,0,0)^T$ which is clearly a self-trapping case.

(ii) When the initial amplitude is $(0,1,0,0)^T$, final light amplitude will be $(0,\frac{1}{2}(e^{i\eta_3}+e^{i\eta_4}),0,\frac{1}{2}(e^{i\eta_3}-e^{i\eta_4}))^T$. It is evident that initial light in the 2nd WG will be divided into the 2nd and 4th WGs and the amount of light energy present in these WGs depends upon the phase factors η_3 and η_4. In particular for $\eta_3=\eta_4$, the light will be completely trapped in the2nd WG (self-trapping case).

(iii) Elementary light amplitude $(0,0,1,0)^T$ leads to the final amplitude given by $(0,\frac{1}{2}(e^{i\eta_3}-e^{i\eta_4}),0,\frac{1}{2}(e^{i\eta_3}+e^{i\eta_4}))^T$. Thus initial light in the 3rd WG will be shared into the 2nd and 4th WGs. In particular when, $\eta_3=\eta_4$, the light will be completely transferred from the 3rd WG to 4th WG. Thus it is obviously a case of light switching.

(iv) If the initial light distribution is $(0,0,0,1)^T$, it leads to a final light distribution given by $(0,0,-e^{i\eta_2},0)^T$ which is a case of power switching from the 4th to the 3rdWG.

Thus our four WG coupler configuration is capable to exhibit power splitting, self-trapping and switching phenomena under different initial light distribution conditions owing to some specific system parameters.

2.1.2 Case 2

We may engineer the coupling coefficients in a manner in which $k_{23}(z)$ precedes $k_{24}(z)$ and $k_{24}(z)$ precedes $k_{12}(z)$. Such sequence of coupling can be mathematically represented by the following asymptotic relations:

$$\vartheta_i(z=-\infty)=0,\vartheta_f(z=+\infty)=\frac{\pi}{2},\phi_i(z=-\infty)=0,\phi_f(z=+\infty)=\frac{\pi}{2}.$$

(i) Now if we envisage the elementary amplitude as $(1,0,0,0)^T$, the final light amplitude will be $(0,0,0,-e^{i\eta_1})^T$. It is clearly a switching case in which light is absolutely transferred from 1st to 4th WG.

(ii) When the initial light sharing is given as $(0,1,0,0)^T$, ultimate light amplitude will be represented by $(0,\frac{1}{2}(e^{i\eta_3}-e^{i\eta_4}),0,\frac{1}{2}(e^{i\eta_3}+e^{i\eta_4}))^T$. It is evident that initial light in the 2nd WG will be shared into the 2nd and4th WGs and the phase factors η_3 and η_4 regulates the light energy content in these WGs. Specifically, for $\eta_3=\eta_4$, the light will be completely shifted into the 4th WG (switching case).

(iii) Final light amplitude will be $(0,\frac{1}{2}(e^{i\eta_3}+e^{i\eta_4}),0,\frac{1}{2}(e^{i\eta_3}-e^{i\eta_4}))^T$ for initial light distribution $(0,0,1,0)^T$. Thus initial light in the 3rd WG will be split into the 2nd and 4th WGs. For $\eta_3=\eta_4$, the light will be completely transferred from the 3rd WG to the 2nd WG.

(iv) If the initial light sharing is $(0,0,0,1)^T$, it directs to a final energy distribution $(0,0,-e^{i\eta_2},0)^T$ which is the case of power switching from the 4th to the 3rdWG.

2.1.3 Case 3

As an alternative, we may fix up the coupling coefficients in a way in which $k_{24}(z)$ precedes $k_{23}(z)$ and $k_{23}(z)$ precedes $k_{12}(z)$. This physical condition may be represented in terms of the following asymptotic relations:

$\vartheta_i(z=-\infty)=0, \vartheta_f(z=+\infty)=\frac{\pi}{2}, \phi_i(z=-\infty)=\frac{\pi}{2}, \phi_f(z=+\infty)=0$.

(i) Under such order of coupling coefficients, if the initial amplitude is $(1,0,0,0)^T$, the final light amplitude will be $(0,0,-e^{i\eta_1},0)^T$. It is clearly a switching case in which light is entirely transferred from the 1st to the 3rdWG.

(ii) Final light amplitude takes the form $(\frac{1}{2}(e^{i\eta_3}-e^{i\eta_4}),\frac{1}{2}(e^{i\eta_3}+e^{i\eta_4}),0,0)^T$ for the initial amplitude $(0,1,0,0)^T$. It is manifested that initial light in the 2nd WG will be split into the 2nd and 1st WG and the percentage of light in these WGs figures on the phase factors η_3 and η_4. Perfect trapping of light in the 2nd WG occurs particularly for $\eta_3=\eta_4$ (self-trapping case).

(iii) For elemental light amplitude $(0,0,1,0)^T$, final amplitude will be $(0,0,0,-e^{i\eta_2})^T$ which indicates that there will be complete switching of light from the 3rd to the 4th WG.

(iv) When we employ the initial amplitude as $(0,0,0,1)^T$, final light amplitude assumes the form $(\frac{1}{2}(e^{i\eta_3}+e^{i\eta_4}),\frac{1}{2}(e^{i\eta_3}-e^{i\eta_4}),0,0)^T$. It is clear that initial light in the 4th WG will be split into the 2nd and 1st WGs and the content of light energy in these WGs depends upon the phase factors η_3 and η_4. In particular for $\eta_3=\eta_4$, the light will be completely shifted into the 1st WG (switching case).

2.1.4 Case 4

In fine, we engineer the coupling coefficients in a manner that the coupling coefficients $k_{24}(z)$ and $k_{23}(z)$ coincide and precede $k_{12}(z)$. Such type of coupling sequences satisfy the following asymptotic relations: $\vartheta_i(z=-\infty)=0, \vartheta_f(z=+\infty)=\frac{\pi}{2}, \phi_i(z=-\infty)=\phi_f(z=+\infty)=\frac{\pi}{4}$.

(i) If we introduce the initial amplitude as $(1,0,0,0)^T$, the final light amplitude will be $(0,0,-\frac{1}{\sqrt{2}}e^{i\eta_1},-\frac{1}{\sqrt{2}}e^{i\eta_1})^T$. It is clearly a power splitting case in which light in the 1st WG is equally transferred to the 3rd and 4th WGs.

(ii) Elementary light amplitude $(0,1,0,0)^T$ leads the final amplitude $(\frac{1}{2}(e^{i\eta_3}-e^{i\eta_4}),\frac{1}{2}(e^{i\eta_3}+e^{i\eta_4}),0,0)^T$. Obviously initial light in the 2nd WG will be shared into the 2nd and 1st WGs and the amount of light in these WGs is ruled by the

phase factors η_3 and η_4. In particular for $\eta_3 = \eta_4$, the light will be completely trapped in the 2nd WG (self-trapping case).

(iii) When the initial amplitude is $(0,0,1,0)^T$, final light amplitude will be $(\frac{1}{2\sqrt{2}}\left(e^{i\eta_3}+e^{i\eta_4}\right),\frac{1}{2\sqrt{2}}\left(e^{i\eta_3}-e^{i\eta_4}\right),\frac{1}{2}e^{i\eta_2},-\frac{1}{2}e^{i\eta_2})^T$ which indicates that initial light in the 3rd WG will be shifted into all the WGs with equal amount of light in the 3rd and 4th WGs (25% in each). Percentage of light shared by the 1st and 2nd WGs figures on the phase factors η_3 and η_4. For $\eta_3 = \eta_4$, 50% (0%) light will be trapped in the 1st (2nd)WG.

(iv) Final light amplitude will be $(\frac{1}{2\sqrt{2}}\left(e^{i\eta_3}+e^{i\eta_4}\right),\frac{1}{2\sqrt{2}}\left(e^{i\eta_3}-e^{i\eta_4}\right),-\frac{1}{2}e^{i\eta_2},\frac{1}{2}e^{i\eta_2})^T$ if we incorporate the initial light amplitude as $(0,0,0,1)^T$. Clearly elemental light in the 3rd WG will be split into all the WGs and the content of light in the 3rd and 4th WGs be equal (25% in each). Percentage of light shared by the 1st and 2nd WGs is governed by the phase factors η_3 and η_4. Specifically for $\eta_3 = \eta_4$, the 50% (0%) light will be trapped in the 1st (2nd)WG.

3. Conclusion

To summarize, the propagation dynamics of a four-WG directional coupler configuration similar to a tripod system in atomic scale is investigated in order to display the optical analogue of coherent population transfer and trapping. Our approach may be treated as a general one in the sense that we have used all the adiabatic states instead of only the dark states (STIRAP technique) responsible for light transfer mechanism. Another important point to highlight is that our system is potent to exhibit double dark resonance. Depending upon the arrangement of various coupling coefficients and different conditions of initial light distribution, the coupler may behave as power splitter, switch and self-trapper etc.

References:

[1] D. Dragoman and M. Dragoman, *Quantum-Classical Analogies* (Springer, Berlin, 2004).

[2] S. Longhi, *Laser and Photon. Rev.* **3** (2009) 243.

[3] S. Longhi, *Phys. Lett. A* **359** (2006) 166.

[4] S. Longhi, G. Della Velle, M. Ornigotti and P. Laporta, *Phys. Rev. B* **76** (2007) 201101(R).

[5] G. Della et al., *Appl. Phys. Lett.* **92** (2008) 011106.

[6] S. Longhi, *Phys. Rev. A* **78** (2008) 013185.

[7] S. Longhi, *J. Mod. Opt*. **56** (2009) 729.

[8] I. Bayal, P. Panchadhyayee, B.K. Dutta and P.K. Mahapatra, *J. Mod. Opt*. **59** (2012) 226.

[9] I. Bayal, P. Panchadhyayee and P.K. Mahapattra, *J. Mod. Opt*. **62** (2015) 1412.

[10] H. Haus, *IEEE J. Quantum Electron*. **17** (1981) 2321.

[11] A.W. Snyder and J.D. Love, *Optical WG Theory* (London, U.K.: Chapman & Hall, 1995).

[12] W.P. Huang and H.A. Haus, *J. Lightwave Techno*. **7** (1989) 920.

[13] N.H. Sun et al., *J. Lightwave Techno*. **15** (1997) 2301.

[14] D. Marcuse, *Bell Syst. Tech. J*. **52** (1973) 817.

[15] K. Iwasaki, S. Kurazono and K. Itakura, *Electron. Commun. Japan*, **58**-C (1975) 100.

[16] R.G. Peall and R.R.A. *Syms, IEEE J. Quantum Electron*. **25** (1989) 729.

[17] C.M. Kim and Y.J. Im, *IEEE J. Select. Top. Quant. Electron*. **6** (2000) 170.

[18] G.J. Liu, B.M. Liang, Q. Li and G.L. Jin, *Opt. Engg*. **42** (2003) 2930.

[19] E. Paspalakis, *Opt. Commun*. **258** (2006) 30.

[20] V.M. Schneider and H.T. Hattori, *IEEE J. Quant. Electron*. **36** (2000) 923.

[21] V.M. Schneider and H.T. Hattori, *Opt. Commun*. **187** (2001) 129.

[22] H.S. Hristova et al., *Phys. Rev. A* **93** (2016) 033802.

[23] I. Bayal, B.K. Dutta, P. Panchadhyayee, P.K. Mahapattra, *Opt. Engg*. **52** (2013) 054003.

Scientific Voyage
Vol. 2, No. 1,
Page 39-49 (2021)

SCIENTIFIC VOYAGE
ISSN: 2395-5546

GCECT
Publication
Jan.-Mar.

Study of physical parameters of the cosmological models of the universe in plane symmetric space-time in modified gravity

Avinash Aman[1]

Microsoft India (R & D) Pvt Ltd., Building 3 Gachibowli Hyderabad, Telangana 500032, India

Abstract: In this paper, we have intended to study the dynamics of the anisotropic universe in modified gravity using the functional $f(R,T)$ in the form $f(R,T) = \lambda R + \lambda T$. The cosmological models are constructed using the volumetric exponential expansion in Bianchi type VI_h (BVI_h) universe for three different values of $h = -1, 0, 1$. The physical behaviors of the models are also studied.

Keywords: Modified Gravity; Perfect Fluid; Deceleration Parameter

1. Introduction

Since the beginning, there has been many significant accomplishments in the field of astrophysics and space science. Among all of them one of the most substantial achievement is Albert Einstein's general theory of relativity. This theory explains, warping of space-time as being the logic behind the observed gravitational phenomena and gives a complete insight of gravity as a geometric property of space-time. Thus relativity theory has crucial implications in present day astrophysics. Contrary to all, Einstein's general theory of relativity fails to explain the accelerated expansion of the universe. This swift extension of the universe is indicated by the recent cosmological data, which also determines that this accelerated expansion of the universe is due to some energy matter with negative pressure. Cosmologists have termed this energy matter as Dark Energy (DE) whose origin is still a suspense. DE has posed an elementary objection to all the gravitational theories. Introduction of "The Cosmological Constant" by Einstein which gives the energy density value of the vacuum space was a step towards explaining the cosmic acceleration but it encountered frequent problems due to considerable disparity between theory and observations [1]. Thus, in order to account for the cosmic acceleration General Relativity can be altered in contrasting ways. One of the ways which has gained enough praise is by modifying the underlying geometry. This is achieved by replacing the Einstein-Hilbert action through a random function. $f(R)$ gravity (function of Ricci scalar R), $f(T)$ gravity(function of scalar torsion T), $f(G)$ gravity (function of G) and $f(R,T)$ gravity (combined function of R and T) are among the few functions which are used to modify the Einstein-Hilbert action. It is considered that $f(R)$ gravity is the most satisfactory function to realize the cosmic acceleration.

Among the several theoretical models proposed in regard of the dark energy and cosmic acceleration, a few are quintessence (Sahni and Starobinsky [2]; Padmanabhan [3]), cosmological constant (Weinberg [4]; Peebles and Ratra [5]), tachyon field (Padmanabhan [6]; Padmanabhan and choudhury [7]), quintom (Feng et al. [8];

[1] E-mail: avinashbitsian@gmail.com

Guo et al. [9]), Chaplygin gas (Kamenshchik et al. [10]; Bento et al. [11]), holographic models (Wang et al. [12]; Setare and Shafei [13], Setare [14]; Hu and Ling [15]; Kim et al. [16]), phantom energy (Caldwell [17]; Nojiri and Odintosov [18]), k-essence, f-essence etc. On the basis of verification of the above theories, modified gravity has been successful in describing the late accelerated expansion of the universe. Thus, modified gravity nowadays is a topic of great interest. Out of all prospective variants of modified gravity, the $f(R,T)$ gravity theory proposed by Harko et al. [19] is one of the most fascinating theories. In this theory they have generalized the basic $f(R)$ theory by taking the gravitational Lagrangian as a random function of Ricci scalar R and trace of the stress-energy tensor T.

Inspired by the above argument and investigations in modified theories of gravity, in this paper, we offer to study a plane, static and symmetric space time in $f(R,T)$ gravity by considering various functions of $f(R,T)$ as proposed in [19] This paper has been organized as follows: In section 1, introductory discussion on modified gravity was made. In section 2, the field equations of $f(R,T)$ gravity in a static, plane symmetric space time has been derived. Section 3 formulates the field equations for a plane, static and symmetric space-time in $f(R,T)$ gravity considering various cases of $f(R,T)$ i.e. (i) $f(R,T) = R+2f(T)$ (ii) $f(R,T) = f_1(R)+f_2(T)$ (iii) $f(R,T) = f_1(R) + f_2(R)f_3(T)$ and giving the solutions for all the three cases. In section 4 physical and geometrical parameters of the models are defined and discussed along with their graphical plots. Finally conclusions are summarized in the last Section 5.

2. $f(R,T)$ Gravity Theory

In $f(R,T)$ gravity, Hilbert-Einstien type variational principle yields the gravitational field equations. The $f(R,T)$ modified gravity action is given by

$$S = \frac{1}{16\pi}\int f(R,T)\sqrt{-g}d^4x + \int L_m\sqrt{-g}d^4x, \tag{1}$$

where $f(R,T)$ is an arbitrary function of Ricci scalar R, T being the trace of the stress-energy tensor (T_{ij}) of the matter and L_m is the matter Lagrangian density.

The stress-energy tensor of matter is defined as

$$T_{ij} = \frac{-2}{\sqrt{-g}}\frac{\delta(\sqrt{-g}L_m)}{\delta g^{ij}}. \tag{2}$$

We assumed here that the dependence of matter Lagrangian is on the metric tensor g_{ij} rather than its derivatives.

The trace of the energy tensor of matter is given by

$$T = g^{ij}T_{ij}. \tag{3}$$

So in this case the stress-energy tensor of matter is

$$T_{ij} = g_{ij}L_m - 2\frac{\partial L_m}{\partial g^{ij}}. \tag{4}$$

Varying the action S of the gravitation field with respect to the metric tensor components g^{ij}, the field equations of $f(R,T)$ gravity are obtained as follows

$$f(R,T)R_{ij} - \frac{1}{2}f(R,T)g_{ij} + (g_{ij}\Box - \nabla_i\nabla_j)f_R(R,T)$$

$$= 8\Pi T_{ij} - f_T(R,T)T_{ij} - f_T(R,T)\theta_{ij} \tag{5}$$

where

$$\theta_{ij} = -2T_{ij} + g_{ij}L_m - 2g^{\alpha\beta}\frac{\partial^2 L_m}{\partial g^{ij}\partial g^{\alpha\beta}}. \tag{6}$$

Now here $f_R(R,T) = \frac{\partial f(R,T)}{\partial R}$, $f_T(R,T) = \frac{\partial f(R,T)}{\partial T}$, $\Box \equiv \nabla^i\nabla_i$ where ∇^i is the covariant derivative and T_{ij} is the standard matter energy-momentum tensor.

Contraction of Eq. (5) yields

$$f_R(R,T)R + 3\Box f_R(R,T) - 2f(R,T) = 8\pi T - f_T(R,T)(T+\theta) \tag{7}$$

where $\theta = \theta^i_i$. The above Eq. (7) gives a relation between the trace T of energy-momentum tensor and Ricci scalar R.

It can be seen that when $f(R,T) \equiv f(R)$, Eq. (5) yields the field equations of $f(R)$ gravity.

Now using Eq. (6), we get the variation of stress-energy. As there is no unique definition of matter Lagrangian, the matter Lagrangian can be taken as $L_m = p$.

Now using the Lagrangian L_m, the stress-energy tensor of matter is given by

$$T_{ij} = (\rho + p)u_i u_j - pg_{ij}, \tag{8}$$

where u^i=(0,0,0,1) is the four velocity vector in the co-moving coordinate system such that $u^i u_i = 1$ and $u^i\nabla_j u_i = 0$, ρ and p are energy density and pressure of the fluid respectively.

Then using Eq. (6), we obtain the variation of Stress-energy of perfect fluid as

$$\theta_{ij} = -2T_{ij} - pg_{ij}. \tag{9}$$

On the physical nature of the matter field,the field equations also depend through the tensor θ_{ij}.

Hence in the case of $f(R,T)$ gravity depending on the nature of matter source. We obtain several theoretical models for different matter contributions for $f(R,T)$ gravity. Harko et al (2011) gave three classes of model as

$$f(R,T) = \begin{cases} R + 2f(T) \\ f_1(R) + f_2(T) \\ f_1(R) + f_2(R)f_3(T). \end{cases} \tag{10}$$

In this paper we focus on all the three above mentioned cases. Firstly we focus on the first case, i.e., $f(R,T) = R + 2f(T)$ where $f(T)$ is an arbitrary function of Stress-Energy tensor of matter. Now from Eq. (5) we get the field equations of $f(R,T)$ gravity as

$$R_{ij} - \frac{1}{2}Rg_{ij} = 8\pi T_{ij} - 2f'(T)T_{ij} - 2f'(T)\theta_{ij} + f(T)g_{ij}, \tag{11}$$

where prime denotes differentiation with respect to the argument.

In perfect fluid the field equations become

$$R_{ij} - \frac{1}{2}Rg_{ij} = 8\pi T_{ij} - 2f'(T)T_{ij} + [2pf'(T) + f(T)]g_{ij}. \tag{12}$$

Then we focus on the second case, i.e., $f(R,T) = f_1(R) + f_2(T)$ where $f_1(R)$ is an arbitrary function of Ricci Scalar and $f_2(T)$ is an arbitrary function of Stress-Energy tensor of matter. For this case in perfect fluid the field equations develop into

$$f_1'(R)R_{ij} - \frac{1}{2}f_1(R)g_{ij} = 8\pi T_{ij} + f_2'(T)T_{ij} + [f_2'(T)p + \frac{1}{2}f_2(T)]g_{ij}. \tag{13}$$

Finally we focus on the third case, i.e., $f(R,T) = f_1(R) + f_2(R)f_3(T)$ where $f_1(R)$ and $f_2(R)$ is an arbitrary functions of Ricci Scalar and $f_3(T)$ is an arbitrary function of Stress-Energy tensor of matter. For this case in perfect fluid the field equations develop into

$$[f_1'(R) + f_2'(R)f_3(T)]R_{ij} - \frac{1}{2}f_1(R)g_{ij}$$

$$= 8\pi T_{ij} + f_2(R)f_3'(T)T_{ij} + f_2(R)[f_3'(T)p + \frac{1}{2}f_3(T)]g_{ij}. \tag{14}$$

3. Field Equations and its solutions

We have considered a static, plane and symmetric space-time of the form

$$ds^2 = A^2(dt^2 - dx^2) - B^2(dy^2 + dz^2), \tag{15}$$

where A(t) and B(t) are the two anisotropic directions of the space and functions of cosmic time only.

These functions are not equal due to radial asymmetry. The matter tensor can be defined as

$$\theta_{ij} = -2T_{ij} - pg_{ij} = (\rho, -p, -p, -p). \tag{16}$$

Now the formulation of equations and their solution for each of the three cases are shown.

3.1 Case I:

$$f(R,T) = R + 2f(T). \tag{17}$$

With specific function choice $f(T) = \lambda T$, where λ is a constant, the field equations are obtained as

$$\frac{2\ddot{B}}{A^2B} + \frac{\dot{B}^2}{A^2B^2} - \frac{2\dot{A}\dot{B}}{A^3B} = (8\pi + 3\lambda)p - \lambda\rho, \tag{18}$$

$$\frac{\ddot{B}}{A^2B} - \frac{\dot{A}^2}{A^4} + \frac{\ddot{A}}{A^3} = (8\pi + 3\lambda)p - \lambda\rho, \tag{19}$$

$$\frac{\ddot{B}}{A^2B} - \frac{\dot{A}^2}{A^4} + \frac{\ddot{A}}{A^3} = (8\pi + 3\lambda)p - \lambda\rho, \tag{20}$$

$$\frac{2\dot{A}\dot{B}}{A^3B} + \frac{\dot{B}^2}{A^2B^2} = -(8\pi + 3\lambda)\rho - \lambda p, \tag{21}$$

where an overhead dot represents differentiation with respect to cosmic time 't'.

As Eqs. (19) and (20) are same, therefore we have four unknowns namely A, B, p, ρ and three equations. Without loss of generality we take

$$A = B^m, \tag{22}$$

where 'm' is an arbitrary constant.

On solving the above Eqs. (18) - (22) we get the solution as

$$A = (k_1 t + k_2)^{m/2}, \tag{23}$$

$$B = (k_1 t + k_2)^{1/2}, \tag{24}$$

where k_1 and k_2 are arbitrary constants. p and ρ for this case are obtained as

$$p = \rho = \frac{-(2m+1){k_1}^2}{8(4\pi+\lambda)(k_1 t + k_2)^{m+2}}. \tag{25}$$

3.2 Case II:

$$f(R,T) = f_1(R) + f_2(T). \tag{26}$$

With specific function choice $f_1(R) = \lambda R$ and $f_2(T) = \lambda T$, where λ is a constant, the field equations are obtained as

$$\frac{2\ddot{B}}{A^2 B} + \frac{\dot{B}^2}{A^2 B^2} - \frac{2\dot{A}\dot{B}}{A^3 B} = (\frac{8\pi+\lambda}{\lambda} + \frac{1}{2})p - \frac{\rho}{2}, \tag{27}$$

$$\frac{\ddot{B}}{A^2 B} - \frac{\dot{A}^2}{A^4} + \frac{\ddot{A}}{A^3} = (\frac{8\pi+\lambda}{\lambda} + \frac{1}{2})p - \frac{\rho}{2}, \tag{28}$$

$$\frac{\ddot{B}}{A^2 B} - \frac{\dot{A}^2}{A^4} + \frac{\ddot{A}}{A^3} = (\frac{8\pi+\lambda}{\lambda} + \frac{1}{2})p - \frac{\rho}{2}, \tag{29}$$

$$\frac{2\dot{A}\dot{B}}{A^3 B} + \frac{\dot{B}^2}{A^2 B^2} = \frac{p}{2} - (\frac{8\pi+\lambda}{\lambda} + \frac{1}{2})\rho, \tag{30}$$

where an overhead dot represents differentiation with respect to cosmic time 't'.

As Eqs. (28) and (29) are same, therefore we have four unknowns namely A, B, p, ρ and three equations. Without loss of generality we take

$$A = B^m, \tag{31}$$

where 'm' is an arbitrary constant.

On solving the above Eqs. (27) - (31) we get the solution as

$$A = (k_1 t + k_2)^{m/2}, \tag{32}$$

$$B = (k_1 t + k_2)^{1/2}, \tag{33}$$

where k_1 and k_2 are arbitrary constants. For this case p and ρ are obtained as

$$p = \rho = \frac{-\lambda(2m+1){k_1}^2}{4(8\pi+\lambda)(k_1 t + k_2)^{m+2}}. \tag{34}$$

3.3 Case III:

$$f(R,T) = f_1(R) + f_2(R) f_3(T). \tag{35}$$

With specific function choice $f_1(R) = \lambda R$, $f_2(R) = \lambda R$ and $f_3(T) = \lambda T$, where λ is a constant, the field equations are obtained as

$$\frac{2\ddot{B}}{A^2B} + \frac{\dot{B}^2}{A^2B^2} - \frac{2\dot{A}\dot{B}}{A^3B} = \frac{8\pi p}{\lambda + \lambda^2\rho - 3\lambda^2 p}, \tag{36}$$

$$\frac{\ddot{B}}{A^2B} - \frac{\dot{A}^2}{A^4} + \frac{\ddot{A}}{A^3} = \frac{8\pi p}{\lambda + \lambda^2\rho - 3\lambda^2 p}, \tag{37}$$

$$\frac{\ddot{B}}{A^2B} - \frac{\dot{A}^2}{A^4} + \frac{\ddot{A}}{A^3} = \frac{8\pi p}{\lambda + \lambda^2\rho - 3\lambda^2 p}, \tag{38}$$

$$(2\lambda^2\rho+2\lambda^2 p)[\frac{\dot{A}^2}{A^2} - \frac{\ddot{A}}{A} - \frac{2\ddot{B}}{B}] + (\lambda^2 p - \lambda - 3\lambda^2\rho)\frac{\dot{B}^2}{B^2} + (6\lambda^2 p - 2\lambda - 2\lambda^2\rho)\frac{\dot{A}\dot{B}}{AB} = 8\pi\rho A^2, \tag{39}$$

where an overhead dot represents differentiation with respect to cosmic time 't'.

As Eqs. (37) and (38) are same, therefore we have four unknowns namely A, B, p, ρ and three equations. Without loss of generality we take

$$A = B^m, \tag{40}$$

where 'm' is an arbitrary constant.

On solving the above Eqs. (36) - (40), we get the solution as

$$A = (k_1 t + k_2)^{m/2}, \tag{41}$$

$$B = (k_1 t + k_2)^{1/2}, \tag{42}$$

where k_1 and k_2 are arbitrary constants. ρ and p for this case are obtained as

$$\rho = \frac{(\frac{m^2}{2} + \frac{m}{2} + \frac{1}{8})\lambda^3 y^2 + (4\pi m + 2\pi)\lambda y}{(16\pi m + 2\pi)\lambda^2 y - (2m^2 + \frac{5m}{4} + \frac{1}{8})\lambda^4 y^2 - 64\pi^2}, \tag{43}$$

$$p = (\frac{8\pi - m\lambda^2 y}{m\lambda^2 y + \frac{\lambda^2 y}{4} + 8\pi})\rho, \tag{44}$$

where

$$y = \frac{k_1^2}{(k_1 t + k_2)^{m+2}}. \tag{45}$$

4. Physical and Geometrical Interpretations

In this section we define and study the physical and geometrical parameters of our model. All the physical and geometrical parameters discussed below are same for all the three cases. The volume scale factor 'V' and the average scale factor 'R' are obtained respectively as

$$V = \sqrt{(-g)} = A^2B^2 = (k_1 t + k_2)^{m+1}, \tag{46}$$

$$R = V^{1/3} = (k_1 t + k_2)^{\frac{m+1}{3}}. \tag{47}$$

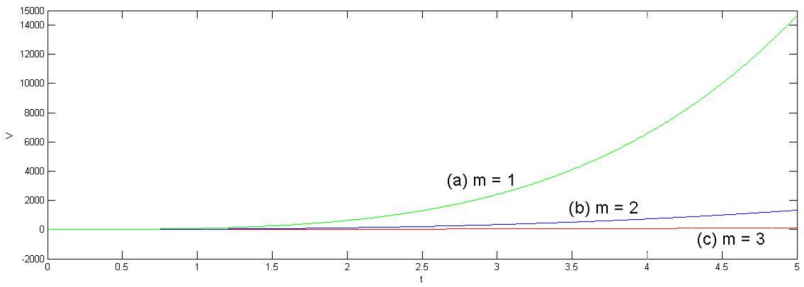

Fig. 1 V versus t for (a) $m = 1$, (b) $m = 2$ and (c) $m = 3$ where $k_1 = 2$, $k_2 = 1$.

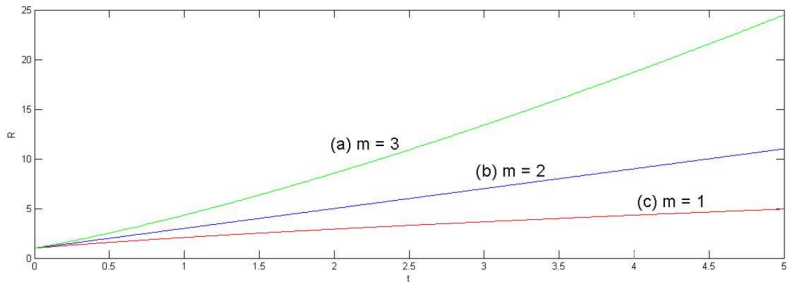

Fig. 2 R versus t for (a) $m = 1$, (b) $m = 2$ and (c) $m = 3$ where $k_1 = 2$, $k_2 = 1$.

The model signifies that the spatial volume increases with increase in time and points out the expanding nature of the space-time. The nature of volume scale factor 'V' and the average scale factor 'R' can be inferred from Figs. 1 and 2 respectively for various values of constant 'm'.

Analogous to this model the scalar expansion 'θ' is given as

$$\theta = \frac{\dot{V}}{V} = \frac{(m+1)k_1}{k_1 t + k_2}. \tag{48}$$

The Hubble parameter 'H' is given as

$$H = \frac{\theta}{3} = \frac{(m+1)k_1}{3(k_1 t + k_2)} \tag{49}$$

which comes out to be a function of 't'.

Measure of the cosmic accelerated expansion of the universe is defined by the deceleration parameter 'q'. Value of the deceleration parameter governs the nature of the space-time. Positive value indicates decelerating model whereas negative value indicates accelerating model. Now, we define the decelerating parameter 'q' as

$$q = \frac{-R\ddot{R}}{\dot{R}^2}. \tag{50}$$

For our model the value of 'q' is obtained as

$$q = -(\frac{m-2}{m+1}). \tag{51}$$

The deceleration parameter attains the following values depending on different values of m

$$q = \begin{cases} > 0 & 0 < m < 2 \\ = 0 & m = 2 \\ < 0 & m > 2. \end{cases} \tag{52}$$

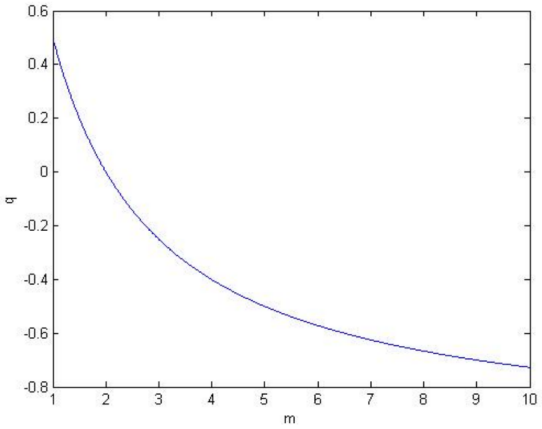

Fig. 3 q vs m where 1 <= m <= 10

Hence the model shows decelerating nature for $0 < m < 2$, remains stagnant at $m = 2$ and accelerating nature for $m > 2$. Behavior of the deceleration parameter 'q' with constant 'm' is shown in Fig. 3.

The Shear scalar 'σ' is defined as follows

$$\sigma^2 = \frac{1}{2}[\sum H_i^2 - \frac{\theta^2}{3}]. \tag{53}$$

For our model it comes out to be

$$\sigma^2 = \frac{(2 - m^2 - 8m)k_1^2}{24(k_1 t + k_2)^2}. \tag{54}$$

The Ricci scalar for all the models is found to be

$$R = (k_1 t + k_2)^{\frac{m+1}{3}}. \tag{55}$$

As t $\to$ 0, R $\to$ $k_2^{\frac{m+1}{3}}$ and as t $\to \infty$, R $\to \infty$. Therefore, it can be seen that the curvature of the space-time is increasing continuously with time and approaches infinity at infinite time. The trace of the stress-energy tensor 'T' for the three cases are respectively as follows

4.1.1 Case I:

$$T = \frac{(2m+1){k_1}^2}{4(4\pi + \lambda)(k_1 \mathrm{t} + k_2)^{m+2}}. \tag{56}$$

4.1.2 Case II:

$$T = \frac{\lambda(2m+1){k_1}^2}{2(8\pi+\lambda)(k_1 t + k_2)^{m+2}}. \tag{57}$$

4.1.3 Case III:

$$T = (\frac{4m\lambda^2 y + \frac{\lambda^2 y}{4} - 16\pi}{m\lambda^2 y + \frac{\lambda^2 y}{4} + 8\pi})\rho, \tag{58}$$

where

$$\rho = \frac{(\frac{m^2}{2} + \frac{m}{2} + \frac{1}{8})\lambda^3 y^2 + (4\pi m + 2\pi)\lambda y}{(16\pi m + 2\pi)\lambda^2 y - (2m^2 + \frac{5m}{4} + \frac{1}{8})\lambda^4 y^2 - 64\pi^2} \tag{59}$$

and

$$y = \frac{k_1^2}{(k_1 t + k_2)^{m+2}}. \tag{60}$$

Now, the function $f(R,T)$ for all the three models are as follows

4.2.1 Case I:

$$f(R,T) = R + 2\lambda T = [(k_1 t + k_2)^{\frac{m+1}{3}} + \lambda \frac{(2m+1){k_1}^2}{2(4\pi+\lambda)(k_1 t + k_2)^{m+2}}]. \tag{61}$$

4.2.2 Case II:

$$f(R,T) = \lambda(R+T) = \lambda[(k_1 t + k_2)^{\frac{m+1}{3}} + \frac{\lambda(2m+1){k_1}^2}{2(8\pi+\lambda)(k_1 t + k_2)^{m+2}}]. \tag{62}$$

4.2.3 Case III:

$$f(R,T) = \lambda R(1+\lambda T) = [\lambda(k_1 t + k_2)^{\frac{m+1}{3}}(1 + \lambda(\frac{4m\lambda^2 y + \frac{\lambda^2 y}{4} - 16\pi}{m\lambda^2 y + \frac{\lambda^2 y}{4} + 8\pi})\rho)], \tag{63}$$

where

$$\rho = \frac{(\frac{m^2}{2} + \frac{m}{2} + \frac{1}{8})\lambda^3 y^2 + (4\pi m + 2\pi)\lambda y}{(16\pi m + 2\pi)\lambda^2 y - (2m^2 + \frac{5m}{4} + \frac{1}{8})\lambda^4 y^2 - 64\pi^2} \tag{64}$$

and

$$y = \frac{k_1^2}{(k_1 t + k_2)^{m+2}}. \tag{65}$$

The geometrical nature of the model is described by the state finder diagnostic pair $\{r, s\}$ which are defined as

$$r = \frac{\dddot{R}}{RH^3} \tag{66}$$

and

$$s = \frac{r-1}{3(q-\frac{1}{2})}. \tag{67}$$

For all the three models discussed above the state finder diagnostic pair $\{r, s\}$ is found to be

$$r = \frac{(m-2)(m-5)}{(m+1)^2} \tag{68}$$

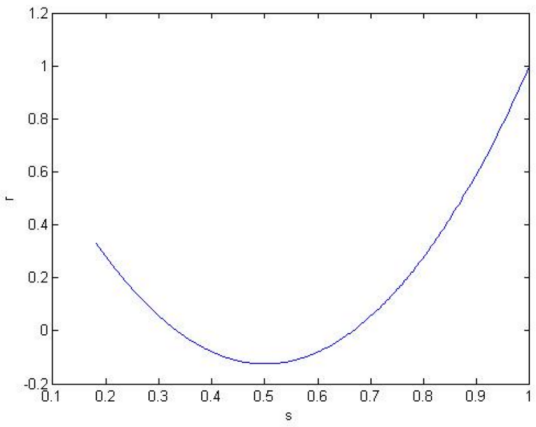

Fig. 4 r vs s where $1 <= m <= 10$

and

$$s = \frac{2}{(m+1)}, \tag{69}$$

where m is an arbitrary constant. Fig. 4 depicts the plot of state finder diagnostic pair r with s.

5. Conclusions

The cosmological models of the universe has been framed in an anisotropic space-time with the three choices of $f(R,T)$ gravity. The dynamical parameters are derived with an assumption between the scale factors. The physical parameters of the models are studied along-with the state finder pair. The models presented here provide a systematic mathematical derivation and the graphical representation shows the physical viability of the model. We conclude that further physical investigations can be performed to get more insight to its behavior.

Acknowledgement

The author is grateful to Prof. B. Mishra, Department of Mathematics, Birla Institute of Technology and Science-Pilani, Hyderabad Campus, Hyderabad 500078, India for his encouragement and constant supervision throughout the work.He also thankfully acknowledges the cooperation that received from the authority of Microsoft India.

References

1. E.J. Copeland et al., *Int J. Mod. Phys. D***15** (2006) 1753.
2. V. Sahnin and A. Starobincsky, *Int. J. Mod. Phys. D* **9** (2000) 373.
3. T. Padmanabhan, *Gen. Rel. Grav.* **40** (2008) 529.
4. S. Weinberg, *Rev. Mod. Phys.* **61** (1989) 1.

5. P.J.E. Peebles and B. Ratra, *Phys. Rev. D* **75** (2003) 559.
6. T. Padmanabhan, *Phys. Rev. D* **66** (2002) 021301.
7. T. Padmanabhan and T. Roy Choudhury, *Phys. Rev. D* **66** (2002) 081301.
8. B. Feng, X.L. Wang and X.M. Zhang, *Phys. Lett. B* **607** (2005) 35.
9. Z.K. Guo, N. Ohta and Y.Z. Zhang, *Phys Rev. D* **72** (2005) 023504.
10. A.Y. Kamemschik, M. Moschella and V. Pasquire, *Phys Lett. B* **511** (2001) 265.
11. M.C. Bento, O. Bertolami and A.A. Sen, *Phys. Rev. D* **66** (2002) 043507.
12. B. Wang, Y. Gong and E. Abdalla, *Phys. Lett. B* **624** (2005) 141.
13. M.R. Setare and S. Shafei, *JCAP* **0609** (2006) 11.
14. M.R. Setare, *JCAP* **0701** (2007) 023.
15. Bo Hu and Yi Ling, *Phys. Rev. D* **73** (2006) 123510.
16. H. Kim, H.W. Lee and Y.S. Myung, *Phys. Lett. B* **632** (2006) 605.
17. R.R. Caldwell, *Phys. Lett. B* **545** (2002) 23.
18. S. Nojiri and S.D. Odintsov, *Phys. Rev. D* **68** (2003) 123512.
19. T. Harko, E.S.N. Lobo, S. Nojiri and S.D. Odintsov, *Phys. Rev. D* **84** (2011) 024024.

Scientific Voyage
Vol. 2, No. 1,
Page 50-51 (2021)

SCIENTIFIC VOYAGE
ISSN: 2395-5546

GCECT
Publication
Jan.-Mar.

BOOK REVIEW

N. R. Sen: Life and Science

Rajinder Singh and Suprakash C. Roy

Shaker Verlag/Düren 2021

Utpal Mukhopadhyay[1]

Satyabharati Vidyapith, Nabapally, North 24 Parganas, Kolkata 700 126, West Bengal, India

Nikhil Ranjan Sen (NRS) is, to some extent, an unsung hero of modern Indian mathematics. In spite of his pioneering work in various branches of Applied Mathematics and pure physics, this person did not receive due recognition in his lifetime and has remained largely obscured in common parlance. It is unfortunate that except publication of some articles on him, none came forward to write an authentic biography of NRS covering his life and scientific contributions. At last, the recently published book *N. R. Sen: Life and Science* by Dr. Rajinder Singh of Oldenberg University, Germany and Suprakash C. Roy, Retired Professor as well as Editor-in-Chief of *Science and Culture*, will fulfill that long felt need. Both Dr. Singh and Prof. Roy are experienced researchers in History of Science and they have several publications, both single and joint. In the book under review, they have unearthed a number of new information about NRS using primary sources. Apart from Introduction, the book contains eight chapters and an Appendix. Of these, six chapters are devoted to discussion of scientific contributions of NRS and his associates.

In **Chapter** 1, family background of NRS, his academic life and connections with various institutions and learned societies like Calcutta Mathematical Society, Indian Statistical Institute, National Institute of Sciences (presently INSA), Indian Science Congress Association etc. have been discussed. The legacy of mathematics culture inherited by NRS and his close relatives has been also demonstrated. It is interesting to note that NRS was a staunch supporter of the opinion that vernacular should be the medium of instruction up to graduate level. **Chapter** 2 deals with early research career and attainment of D.Sc. degree of NRS. The title and examiners of his thesis and usual application seeking permission for submission of the same etc. have been

[1] Email: utpalsbv@gmail.com

discussed in detail. In **Chapter** 3, background of NRS's interest in relativity and his research in Germany under the supervision of two towering figures of physics have been discussed. Doctorate degree conferred on NRS in Germany, the title of his thesis and names of its examiners have also been presented in detail. Research of NRS in relativity after returning to India is also discussed. Cosmological work of NRS, viz. work on de Sitter's universe, Friedmann model, Milne's cosmological view, expansion of nebula etc. are the topics covered in **Chapter** 4.

In **Chapter** 5, investigations done by NRS and his associates on mass, density, radius, temperature, pressure, composition, stability etc. of stars on the basis of Bethe's law of energy generation and Cowling model are presented including work on red giant stars. Study of turbulence and research in fluid dynamics are the major subject matters of **Chapter** 6. In this connection, a summary of the book *The Modern Theory of Turbulence*, written by NRS has been discussed also. In **Chapter** 7, work of NRS and his associates in defence research, viz. work on ballistics including the history of inclusion of the study of ballistics in M. Sc. course and supervision of work on ballistics by NRS are discussed. Works of NRS in wave mechanics, quantum mechanics, glowing metals etc. are also included in this chapter. Some of the posthumous recognitions bestowed on Prof. N. R. Sen and his scientific contributions mentioned by some recent authors have been narrated in **Chapter** 8. In the Appendix, an improved list of papers and books written by NRS has been provided.

A salient feature of the book is that before discussing the contributions of NRS, basic ideas and historical background of the field in which NRS worked have been very lucidly explained along with previous works done in that line of research. This will help the readers to grasp the essence and importance of NRS's work in that particular area. The book contains a number of rare and historical photographs which have enhanced its importance. Moreover, as mentioned by the authors, there still remain some unanswered questions about NRS. So, this book may trigger further research on The Father of Applied Mathematics in India. Finally, it should be mentioned that this book is a must read for the researchers in History of Science as well as common readers interested about the development of mathematics in modern India.